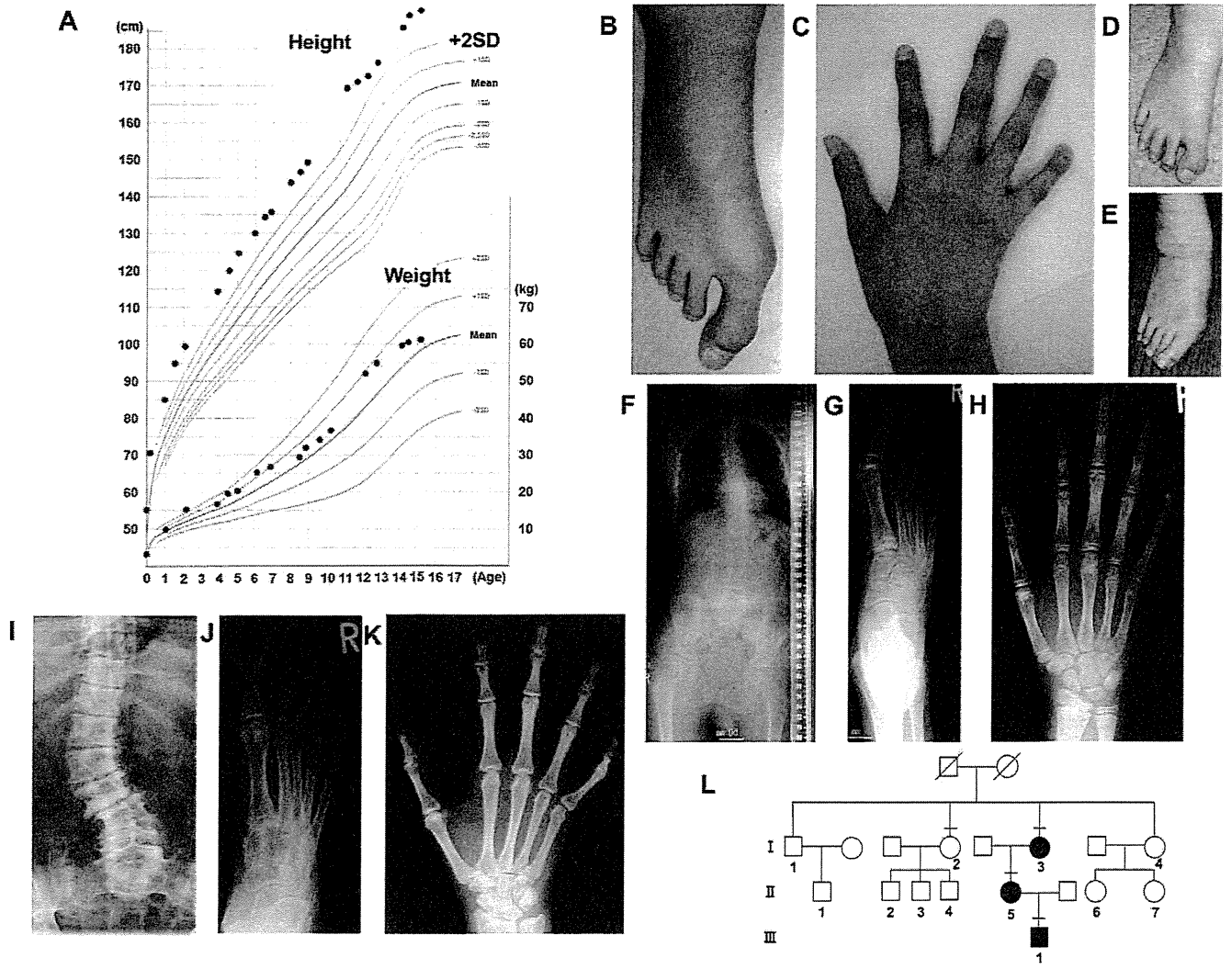


**Figure 1. Clinical manifestations of the family.** (**A**) Growth curve of the proband. The X- and Y- axis indicate age (year) and height (cm) or weight (kg), respectively. The bold line represents the mean for Japanese males. (**B, C**) Photographs of the proband's right foot (B) and hand (C). The great toe was markedly long and wide. The fifth distal phalanx of the hand also showed minor clinodactyly. He has given written informed consent to publication of his photographs. (**D, E**) The right foot of the mother (D) and grandmother (E), respectively. The mother's great toes were surgically shortened at 15 years of age. The grandmother's great toes were large in early life and shortened due to arthrogryposis with aging. They have given written informed consent to publication of their photographs. (**F–H**) Radiographs of the proband's skeleton. His spine showed mild scoliosis (F). The great toe was markedly long and wide (G), and the fifth distal phalanx of the hand showed minor clinodactyly (H). (**I–K**) Radiographs of the mother. Severe scoliosis and lumbar vertebra fractures (I) as well as a markedly long and wide great toe (J), and minor clinodactyly in the fifth digit of the hand (K) were observed, like in the proband. (**L**) Family tree. III-1, II-5, and I-3 indicate the proband, mother, and maternal grandmother, respectively, who had the phenotype. I-2 indicates a maternal grand-aunt, who had no phenotype and was included in the present study.
doi:10.1371/journal.pone.0042180.g001

showed tall stature, scoliosis, and long hands and feet with arachnodactyly of all the fingers and toes, the great toes being markedly long and wide. In addition, the fifth distal phalanx of the hands exhibited minor clinodactyly (Fig. 1B, C). He had no history of cardiac diseases, hypotension, ophthalmic disease, deafness, or digestive system disease. Hematological, biochemical and endocrinological values including insulin-like growth factor-I (IGF-I) were normal. However, bone formation and resorption markers were increased (serum bone-specific alkaline phosphatase, 270 U/l [normal range, 13–33.9]; osteocalcin, 12.5 ng/ml [normal range, 2.9–12.3]; cross-linked C-terminal telopeptide of type I collagen, 14.3 ng/ml [normal range, <4.5]; urinary cross-linked N-telopeptide of type I collagen, 524 nmolBCE/l [normal range, <55]). The bone mineral density (BMD) Z-score of the lumbar spine for $L_{2-4}$, determined with dual-energy x-ray absorptiometry (Discovery A, Hologic), was −1.2, and −3.9 when corrected for his height. Bone age was 11.0 years. Radiological examination of the skeleton showed mild scoliosis, markedly long and wide great toes, and minor clinodactyly in the fifth digit of the hands (Fig. 1F–H). At the age of 15, his height reached 191.2 cm (+3.89 SD), and penile Tanner's stage was IV.

The family tree (Fig. 1L) illustrates that the proband [III-1] has no siblings, and that his mother [II-5] and maternal grandmother [I-3] have the same phenotype (Fig. 1D, E). Clinical manifestations of II-5 were as follows: age, 46 years; height, 176 cm (+3.8 SD for her age); blood pressure, 140/70 mmHg. Her great toes were surgically shortened at 15 years of age. She was given no medication, including antihypertensive drugs. Her menstrual cycles

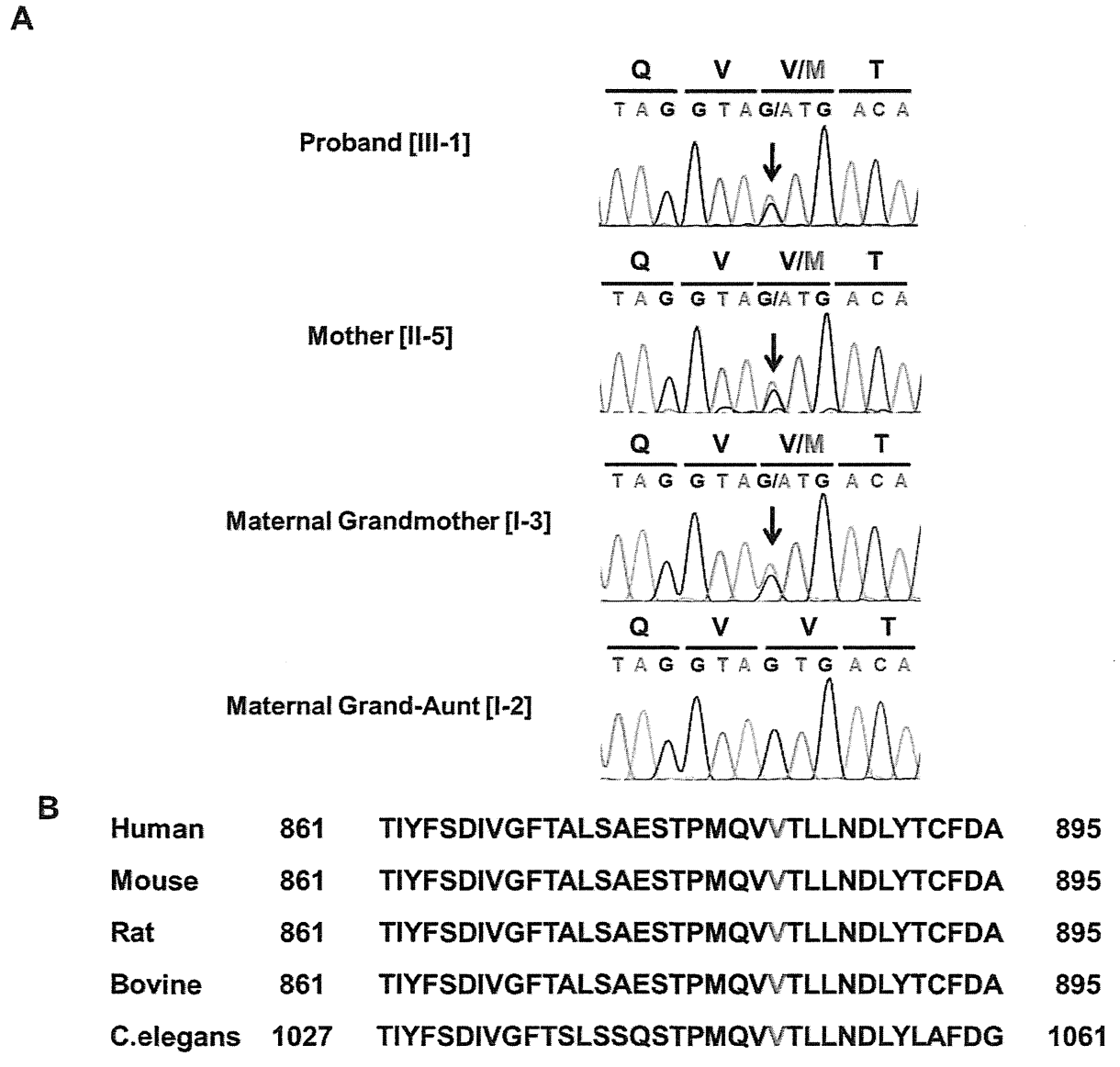


**Figure 2. Identification of the *Npr2* mutation.** (**A**) A novel G→A missense mutation at nucleotide +2647 creates a substitution, methionine for valine, at codon 883 in a heterozygous state in the proband [III-1], mother [II-5], and maternal grandmother [I-3] (arrows). The same position in the maternal grand-aunt without the phenotype [I-2] was not mutated. (**B**)Amino acid alignment of NPR2 among various species. Valine at codon 883 is located in a highly conserved region in the carboxyl-terminal guanylyl cyclase domain of NPR2.
doi:10.1371/journal.pone.0042180.g002

are regular. Radiological examination of II-5 showed severe scoliosis and lumbar vertebra fractures as well as markedly long and wide great toes, and minor clinodactyly in the fifth digit of the hands, like the proband (Fig. 1I–K). The BMD of the lumbar spine for $L_{2-4}$ could not be evaluated due to compressed fractures of the lumbar vertebrae. Clinical manifestations of I-3 were as follows: age, 63 years; height, 166 cm (+3.0 SD for her age); blood pressure, 134/70 mmHg. She underwent right hip replacement arthroplasty at 50 years of age because of degenerative hip disease. She developed hypertension up to 210/110 mmHg at 59 years of age, when antihypertensive therapy was initiated. Her great toes were large in early life and shortened due to arthrogryposis with aging.

## Identification of a Novel Missense Mutation p.Val883Met in the Npr2 Gene

Since the phenotype of the patients most closely resembled several cases of the CNP overproduction phenotype due to a chromosomal translocation, in terms of tall stature and large great toes [9–10], enhanced CNP/NPR2 signaling was suspected. The concentration in serum of amino-terminal pro CNP was slightly decreased in III-1; 3.02±1.15 pmol/l, compared to the control (7.54±1.50 pmol/l). Those in II-5 and I-3 were almost in the normal range; 2.29 and 4.99 pmol/l, respectively, compared to the control subjects (3.53±0.75 pmol/l), ruling out over-production of CNP. Since the proband's phenotype also showed similarity to CATSHL syndrome [13], caused by a loss-of-function mutation in the *Fgfr3* gene, except for the absence of neurological symptoms, the *Fgfr3* gene was analyzed as well as the natriuretic peptide precursor C (*Nppc*), *Npr2*, and *Npr3* genes.

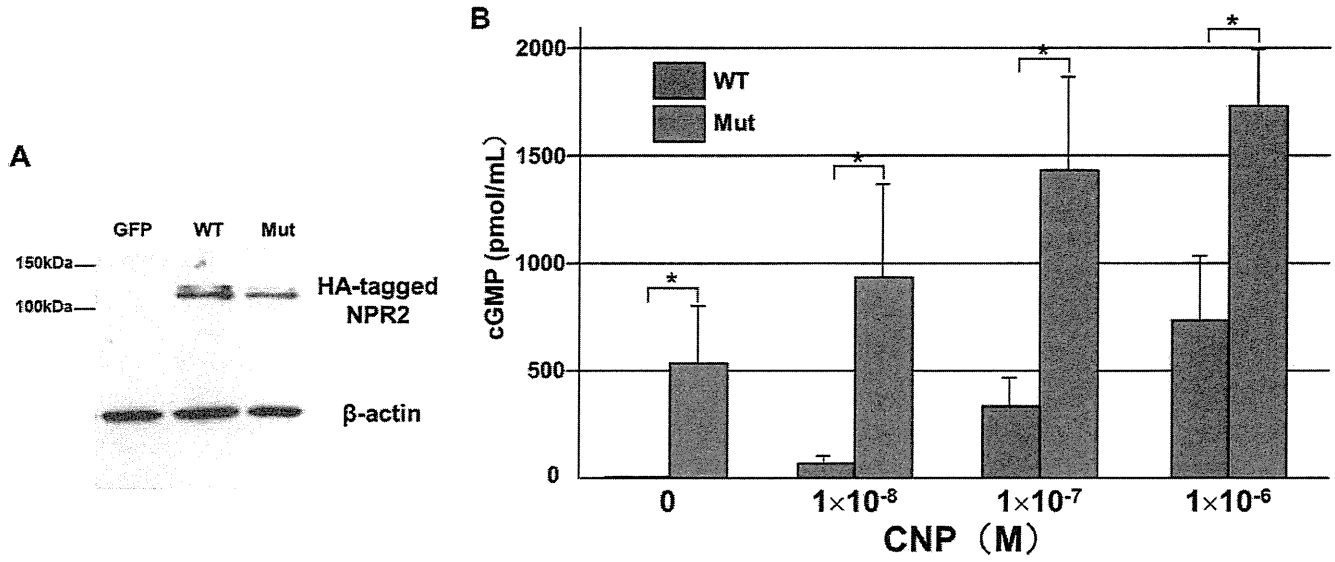


**Figure 3. p.Val883Met is a gain-of-function mutation.** (**A**) Western blot analysis confirmed the comparable expression of HA-WT (WT) and HA-Val883Met (Mut). HEK293A cells were transfected with HA-WT or HA-Val883Met constructs, and lysates were harvested for Western blotting using anti-HA antibody. As an internal control, β-actin in each sample was detected with anti-β-actin antibody. (**B**) Increased cGMP production in the HEK293A cells transfected with the p.Val883Met mutant (Mut) compared to that in wild-type cells (WT). Forty-eight hours after the transfection, the cells were serum-starved for 24 h, and then treated with the indicated concentrations of CNP-22 for 10 min, before cGMP production was assayed. Results are presented as the mean ± SD (N = 3, $*p<0.05$).
doi:10.1371/journal.pone.0042180.g003

We screened these four genes in III-1, II-5, I-3, and a maternal grand-aunt [I-2] who had no phenotype using genomic DNA extracted from peripheral blood leukocytes, and identified a novel heterozygous G→A missense mutation at nucleotide +2647 (c.2647G→A) of the *Npr2* gene in III-1, II-5, and I-3 that creates a substitution of methionine for valine (p.Val883Met), while the same position in I-2 was not mutated (Fig. 2A). This variant was not registered in the dbSNP (http://www.ncbi.nlm.nih.gov/projects/SNP/) and JSNP (http://snp.ims.u-tokyo.ac.jp/) databases nor found in 214 alleles from healthy Japanese controls. Amino acid Val883 is located in a highly conserved region of the carboxyl-terminal guanylyl cyclase domain of NPR2 and is conserved across species (Fig. 2B). No mutations were found in the *Fgfr3*, *Nppc*, and *Npr3* genes.

## Increased Plasma cGMP Concentrations in the Patients

The plasma concentrations of cGMP in 10 healthy adults were 3.1±1.1 pmol/ml. Plasma cGMP concentrations were elevated in III-1, II-5, and I-3; 20.0, 12.0, and 7.3 pmol/ml. Conversely, that in I-2 without the phenotype was 3.6 pmol/ml, which was similar to the values in healthy adults.

## p.Val883Met is a Gain-of-Function Mutation

To investigate the pathogenic significance of the p.Val883Met mutation, an *in vitro* functional assay was performed. HEK293A cells were transfected with the HA-WT and HA-Val883Met constructs, and whole-cell extracts were harvested for Western blotting. The Western blot analysis using anti-HA antibody confirmed that HA-WT and HA-Val883Met were expressed at comparable levels, with an approximate molecular size of 120 kDa (Fig. 3A). cGMP production in the cells expressing HA-WT and HA-Val883Met was also examined. Treatment with CNP-22 at a dose of $1\times10^{-8}$–$1\times10^{-6}$ M increased intracellular cGMP levels in a dose-dependent manner with concentrations always significantly higher in HA-Val883Met-expressing cells than HA-WT-expressing cells ($*p<0.05$) (Fig. 3B). Intriguingly, cGMP was produced in HA-Val883Met-expressing cells even in the absence of CNP, while no production was observed in HA-WT-expressing cells. These results indicate that p.Val883Met is a gain-of-function type mutation.

## Transgenic Expression of the p.Val883Met Mutant Npr2 in Mice Resulted in a Skeletal Phenotype Similar to that Observed in the Patients

Then, we further investigated the effects of p.Val883Met on skeletogenesis by generating transgenic mice expressing the mutant *Npr2* in chondrocytes. Transgenic founder No. 4 exhibited severe bone deformities including elongation of the spine with severe kyphosis, metatarsal bones, and distal phalanges, and died at seven weeks (Fig. 4A). Founder No. 28 also exhibited an elongated tail and toes with mild kyphosis, and could produce offspring mice. The amount of transgene mRNA in cartilage was quantified by real-time PCR and standardized based on the mRNA level of *Sox9*, a marker for chondrocytes. The higher expression of the transgene mRNA was detected in No. 4 than in No. 28 (data not shown).

Then, we evaluated the skeletal phenotype in No. 28 offspring (Tg. 28). First, the expression of *Npr2* was determined using RNA extracted from costal cartilage of Tg. 28 and wild-type littermates (Wt) at 5 days of age. The total amount of *Npr2* mRNA, including native and transgenic *Npr2*, was quantified by real-time PCR and standardized based on the mRNA level of *Gapdh* (Tg. 28, 1.83±0.77; Wt, 0.36±0.08, $*p<0.05$) (Fig. 4B). cGMP concentrations in costal cartilage were also measured (Tg. 28, 102.2±11.3; Wt, 5.9±0.6 pmol/mg DNA, $*p<0.05$) (Fig. 4C). Although the total amount of *Npr2* was 5.1 times higher in Tg. 28 than Wt, the cGMP concentration was 17.3 times higher, supporting the *in vitro* data demonstrating the gain of function of the p.Val883Met mutant NPR2.

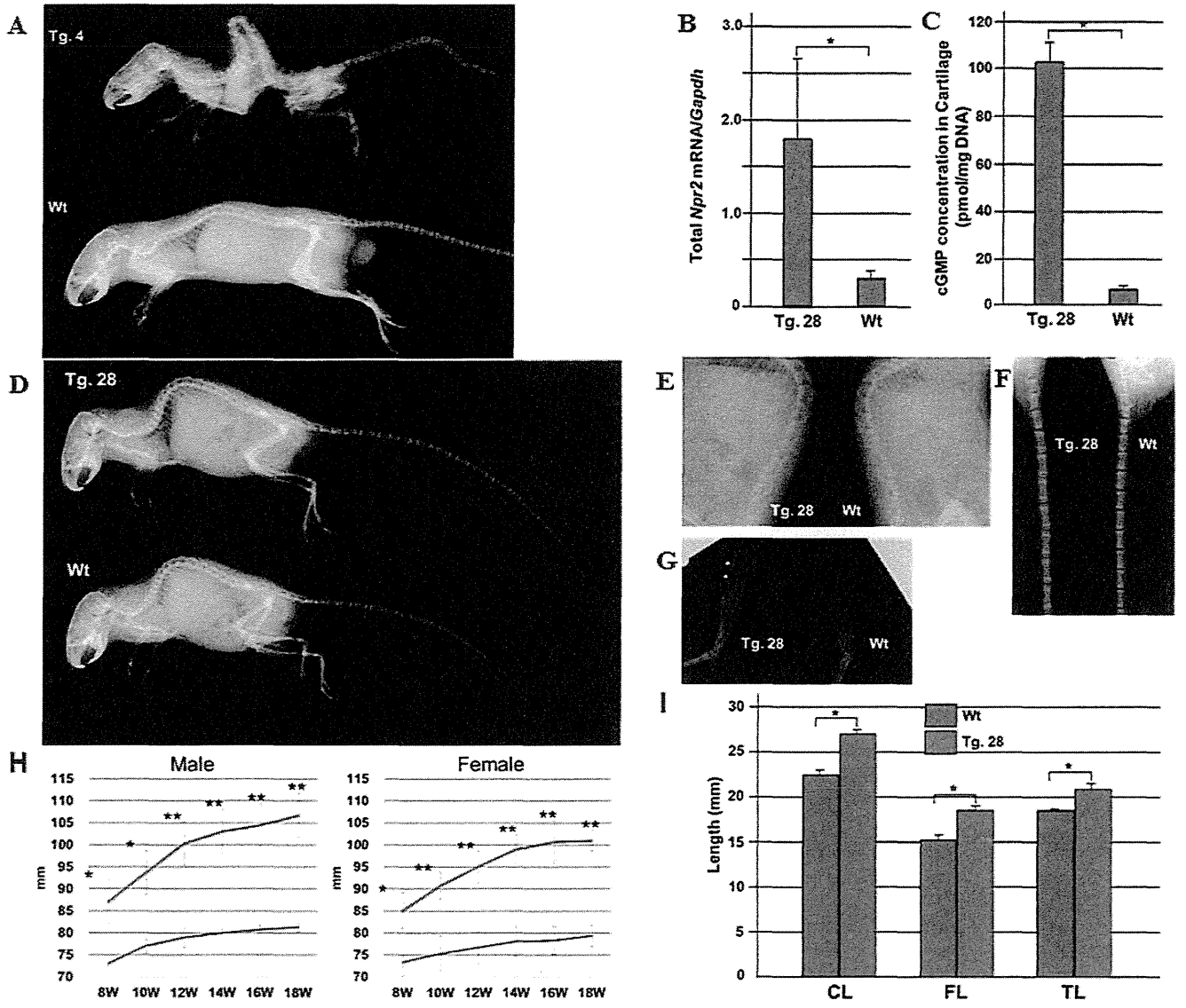


**Figure 4. Transgenic expression of the p.Val883Met mutant in chondrocytes reproduced the patients' phenotype in mice.** (**A**) Radiographs of transgenic founder No. 4 expressing the p.Val883Met mutant NPR2 with the severest phenotype (Tg. 4) and a wild-type mouse (Wt). Tg. 4 exhibited severe bone deformities including elongation of the spine with severe kyphosis, metatarsal bones and distal phalanges, and died at seven weeks of age. (**B**) The total amount of *Npr2* mRNA in costal cartilage of line No. 28 offspring (Tg. 28) and wild-type littermates (Wt) at 5 days of age. The expression of *Npr2* mRNA in Tg. 28 was 5.1 times that in Wt. Results are presented as the mean ± SD (N = 3, *$p<0.05$). (**C**) Concentration of cGMP in costal cartilage of Tg. 28 and Wt at 5 days of age. The cGMP concentration in Tg. 28 was 17.3 times that in Wt. Results are presented as the mean ± SD (N = 3, *$p<0.05$). (**D–G**) Radiographs of Tg. 28 with a moderate phenotype and Wt at the age of 8 weeks. Body length, defined as the distance between the incisor and the anus, was longer in Tg. 28 than Wt. Total tail length was also longer in Tg. 28. The length of spinal (E) and tail (F) vertebrae was longer in Tg. 28 as well. All the metatarsal bones and distal phalanges were longer in Tg. 28 than Wt (G, arrows), and minor clinodactyly was detected, (**H**) The tail length of Tg. 28 (red line) and Wt (blue line) from 8 to 18 weeks. Tail length was always significantly longer in Tg. 28 than Wt among both males and females. Results are presented as the mean ± SD (N = 3, *$p<0.05$, ** $p<0.001$). (**I**) Bone length of Tg. 28 and Wt (18 week-old males). CL, Naso-occipital length of the calvarium; FL, femoral length; TL, tibial length. Results are presented as the mean ± SD (N = 3, *$p<0.05$).
doi:10.1371/journal.pone.0042180.g004

Representative radiographs of Tg. 28 (female, 8-week-old) are shown in Fig. 4D–G. The spinal and tail vertebrae and phalanges were longer in the transgenic mouse than Wt, indicating the longitudinal overgrowth of bones. Body length (data not shown) and tail length (Fig. 4H) were significantly longer in Tg. 28 than Wt from 8 to 18 weeks. In adulthood, Tg. 28 came to exhibit severe kyphosis and claudication in the legs, resembling the symptoms observed in patient I-3 and transgenic founder No. 4. In addition, naso-occipital length of the calvarium, femoral length, and tibial length were significantly longer in Tg. 28 than Wt at 18 weeks (*$p<0.05$) (Fig. 4I). Thus, the transgenic mice exhibited the skeletal overgrowth associated with the overproduction of cGMP in cartilage.

## Transgenic Mice Expressing the p.Val883Met Mutant Npr2 Exhibited Wider Growth Plates than Wild-type Littermates

Histological examination of the femora and tibiae in 8-week-old mice revealed that Tg. 28 had wider growth plates than Wt

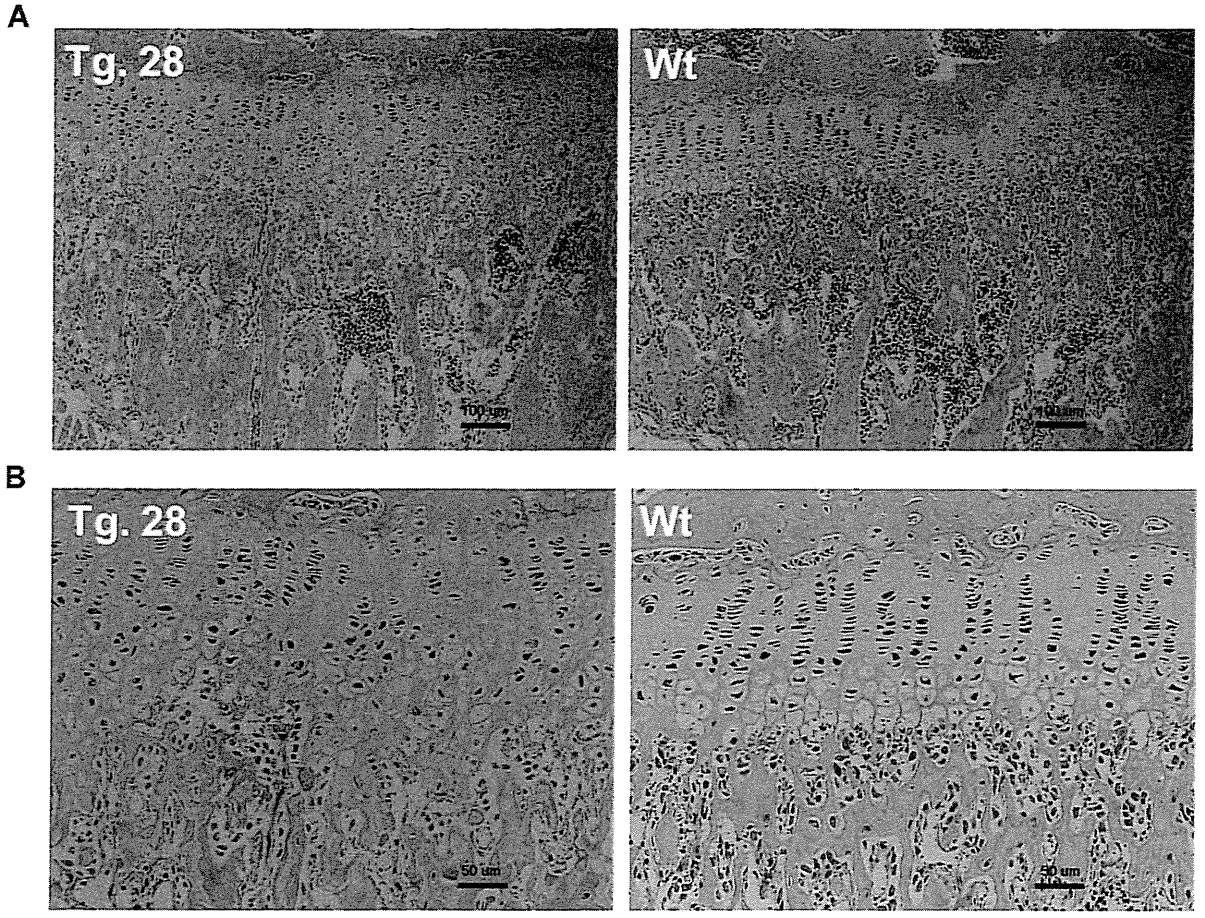


**Figure 5. Hematoxylin-eosin-stained sections of growth plates of Tg. 28 and Wt at 8 weeks of age.** The magnifications are ×40 (scale bar = 100 nm) and ×200 (scale bar = 50 nm) in (A) and in (B), respectively.
doi:10.1371/journal.pone.0042180.g005

(Fig. 5A). At higher magnification, a disorganized arrangement of chondrocytes with increased number of hypertrophic chondrocytes was observed in Tg. 28 (Fig. 5B).

## Discussion

Here we have described a three-generation family with tall stature and macrodactyly due to a newly identified gain-of-function mutation of the *Npr2* gene, p.Val883Met. Increased levels of cGMP both in blood samples of the patients and whole cell lysates expressing the mutant receptor clearly indicate its hypermorphism. Transgenic mice in which p.Val883Met mutant NPR2 was expressed in chondrocytes exhibited the elevated cGMP concentration and the excessive growth and deformities of vertebrae and long bones, which reproduced the symptoms observed in the patients. Taken together, our data are compatible with the interpretation that p.Val883Met mutant is constitutively active and causes skeletal overgrowth by increasing the level of cGMP in chondrocytes. However, we cannot exclude the possibility that the high expression level of NPR2 also contributed to overgrowth in transgenic mice to some extent.

Histological examination confirmed that the skeletal overgrowth was caused by the widening of the growth plates in the transgenic mice expressing the mutant *Npr2* (Fig. 5). As expected, the histological finding was similar to, but severer than, that reported in the mice with overexpression of CNP in chondrocytes [14]. The disorganized arrangement of chondrocytes in the transgenic mice indicates the critical role of the CNP/NPR2 pathway in chondrogenesis. Interestingly, the number of hypertrophic chondrocytes appeared to be increased in the transgenic mice,

**Table 1.** Primer sets for the human *Nppc* gene.

| | Primer sequence (5′→3′) | | |
|---|---|---|---|
| Exon | Forward | Reverse | Product size (bp) |
| 1 | GATTATAAAGGCGCGAGCAG | CTGCCTTCCCTCTCTCCTG | 366 |
| 2 | CTTGGGAGGGACACCCC | CACAACTTGAGCAAAGGCG | 517 |

doi:10.1371/journal.pone.0042180.t001

**Table 2.** Primer sets for the human *Npr2* gene.

| | Primer sequence (5′→3′) | | |
|---|---|---|---|
| Exon | Forward | Reverse | Product size (bp) |
| 1–1 | CTGTAGGCCAGAGCAGCC | AACCAGAGGCCACAGCAC | 441 |
| 1–2 | GACCCCGACCTGCTGTTAG | AGCTTTAGGGACACAGCGAC | 454 |
| 2 | GGGACATCCCAGTGATTCAG | ACAATTCCTGCCTGGTTCC | 397 |
| 3 | AAGTTTCCCTGTCCTGCATC | AGAGAAGCCCTTCCCCAAAG | 253 |
| 4, 5 | ACCCCAGAGAGAGGGGAAG | ACTGAACCCTTGAAAGCTGG | 593 |
| 6, 7 | GAAACAGCTGGGGTCTGG | CTTCAGCCAGAGGTTGTGTG | 581 |
| 8, 9 | AACCCTGCTGTTGGCTTG | GATGGGGATGAGACAGGATG | 484 |
| 10, 11 | CCACTGCTCTCTAGCATTTCC | CAGTATAACTTTGGGTCTATCCTTCC | 540 |
| 12 | ATGCTGGGTGATAGCTGGTG | CCACAATCAAAGAACAGTGGAAG | 196 |
| 13, 14 | AGCTAGCCAGTGCCCATCTC | TCTCTGAGGGTGATCAAAGG | 640 |
| 15, 16 | TACCCACAGCCTCTTCTTCC | GATGAGGCAGAGCCCAAC | 602 |
| 17, 18 | TGCAGCCACATACACTTTCC | TGAGTTTCAAAGCGGGTCTC | 516 |
| 19, 20 | GTGTCAAGCTTGTCTCCCTC | GGGATTATGAAAAGAAGAAAAGGG | 496 |
| 21, 22 | TCGGGCACGGTGCTATAC | GTGTGTGCAGACATGGTGG | 458 |

doi:10.1371/journal.pone.0042180.t002

suggesting the involvement of CNP/NPR2 pathway in chondrocyte differentition.

Although NPR2 is expressed in various tissues, the phenotype seems to be confined to cartilage and bone in humans, as suggested by the clinical manifestations of our patients. It is worth noting that the transmission of the mutant *Npr2* gene seems to have had no apparent effect on fertility in the family, although infertility was observed in *Nppc* or *Npr2* null or hypomorphic mice [7,15].

The second messenger cGMP is generated by two distinct types of guanylyl cyclases; cytoplasmic (soluble) and membrane-bound [16]. The two types share a similar catalytic domain which is conserved from bacteria to humans [17–18]. Seven mammalian membrane-bound guanylyl cyclases have been identified, consisting of ligand-binding, kinase homology, dimerization, and guanylyl cylase domains [4]. ANP, BNP, CNP, and intestinal peptides such as guanylin and uroguanylin have been identified as ligands for the membrane-bound guanylyl cylases. Although a few constitutively activate guanylyl cyclases were synthesized by chemical methods [19], p.Val883Met is the first gain-of-function mutation of NPR2 in living beings. Since cGMP is an important second messenger of several bioactive factors, cGMP-related drugs such as inhibitors of cyclic nucleotide phosphodiesterase have been developed. Erectile dysfunction, pulmonary dysfunction, cardiomyopathy, headache, dementia, and cancer are the targets of treatment with drugs that increase cGMP levels. However, drugs that directly activate guanylyl cylases have not been developed, with the exception of BAY 63-2521 (riociguat) [20]. The amino acid Val883 is located in the catalytic domain and preserved across species. The mechanism of activation in the mutant is beyond the scope of this paper, but the substitution may facilitate a conformational change in the catalytic domain, and in future, an analysis of the higher-order structure of the mutant protein may lead to the development of new drugs stimulating production of cGMP *in vivo*.

In conclusion, we have identified a gain-of-function mutation of *Npr2* in a family with tall stature and macrodactyly. Our findings reconfirm a critical role for NPR2 in skeletal growth in both humans and mice, and may provide a potential target for

**Table 3.** Primer sets for the human *Npr3* gene.

| | Primer sequence (5′→3′) | | |
|---|---|---|---|
| Exon | Forward | Reverse | Product size (bp) |
| 1–1 | AAGAGTGGGGAGGAAAGAGG | ACTGGCGCTGCTGCATAC | 512 |
| 1–2 | CTTCAGCTTGGTGGACCG | CTGCAGAGTGGACGAGTGTG | 513 |
| 2 | TGCTAGGTTCCTCCATGGTC | CACCACCCCTAGAAGTCCC | 599 |
| 3 | GAATGGCCTCTTTATGGTGG | AATGGCTCAGAATGGGACAC | 318 |
| 4 | CCTGGCATGAGTCACTTGG | CAGCTGCAACTGAGAAATACAG | 272 |
| 5 | TTTTGTTGGCAGACAGAGG | CAAATGCATTCCTCAGAGTCC | 225 |
| 6 | GGAATAGCTGTGGAAGGCTG | CTTACATTACACTGAGGTTAGAGGTG | 276 |
| 7 | CTCCAATGGGAAATCGAGG | CTGGGTGAAAGAGGGATGTG | 293 |
| 8 | AAGAGAAACCATGGTATTTTGTAGC | CATTGATGTCTTTCAACCCG | 246 |

doi:10.1371/journal.pone.0042180.t003

**Table 4.** Primer sets for the human *Fgfr3* gene.

| Exon | Primer sequence (5′→3′) | | |
|---|---|---|---|
| | Forward | Reverse | Product size (bp) |
| 1 | CGAGGGGGCGTGCCCTGCGCC | AGCACCGTTGGACCCCTCCG | 339 |
| 2 | AGGGGTCGGGACGCAGGAG | CCCAACGCCTCTGCCCGCAC | 350 |
| 3 | GTCTGTAAACGGTGCCGG | ACCAGAGAGACCCCCAGC | 425 |
| 4 | ATCTGGGAGGGGCACCTGGG | GTCCCTCAGCTGCCTGTGAAG | 222 |
| 5 | GTTCAGAGGGGCCTCTGCTC | AGTGAGCGGAGGCAGCAACC | 290 |
| 6, 7 | CTGCCTCCGCTCACTCAC | GAAGCTCCAACCCCTAGACC | 554 |
| 8 | TCTCCCACATCCTGCCTC | GGGCCTTGGAGCTGGAGCTC | 277 |
| 9 | AGGGCGGTGCTGGCGCTCGC | AGACAGTGCGGAGCAGCAGC | 228 |
| 10 | CAGGCCAGGCCTCAACGCCC | AGGCCTGGCGGGCAGGCAGC | 271 |
| 11 | CTGTACCTCCACGCCCTGTCGC | CTGTTTCACCCCCACCACC | 264 |
| 12 | GAGTGGGCGAGTTTGCACACTC | GTGCAGAGCAGGGCTGGGGGC | 211 |
| 13 | GTGCAGAGCAGGGCTGGGGGC | GCTCCTCAGACGGGCTGCCAG | 240 |
| 14 | CTGGCAGCCCGTCTGAGGAGC | CTGCTCCCAGCATCTCAGGGCA | 286 |
| 15 | GGTGGAGAGGCTTCAGCCCT | GCCAGGCGTCCTACTGGCATGA | 217 |
| 16 | TCATGCCAGTAGGACGCCTGGC | GGTCCTGGCTCTGCCCAGTTC | 184 |
| 17 | CAGCGCAGCCCTGGCCTATTC | CCTGAAGGGCTGCCAGTCCCT | 314 |
| 18 | GAAGCGGCGGGGCTCACTCCT | ATAGGCGGGTGGCACCAGGC | 180 |
| 19 | GCGAAGAGGGGCTCGGTGGCAC | CACCAGCAGCAGGGTGGGCTGCTAG | 254 |

doi:10.1371/journal.pone.0042180.t004

prevention and treatment of diseases caused by impaired production of cGMP.

## Materials and Methods

### Mutation Analysis

The mutation analysis was approved by the ethics committee at Osaka University Graduate School of Medicine, and written informed consent was obtained from the proband and family members for the analysis of the natriuretic peptide precursor C (*Nppc*), *Npr2*, *Npr3* and *Fgfr3* genes.

All the exons of the 4 genes were amplified using specific primers flanking the intron-exon boundaries according to published human *Nppc*, *Npr2*, *Npr3*, and *Fgfr3* genomic DNA sequences (UCSC genome browser: uc002vsl.1 at chromosome 2, 232498379–232499203; uc003zyd.1 at chromosome 9, 35782406–35799728; uc003jhv.2 at chromosome 5, 32711665–32787252; uc003gds.2 at chromosome 4, 1764337–1780396, respectively). Two primers for the *Nppc* gene, 14 primers for the *Npr2* gene, 9 primers for the *Npr3* gene, and 18 primers for the *Fgfr3* gene were designed using the software Primer3Plus and synthesized to cover the genomic sequence from the start codon to the termination codon. The sequences of the primers are provided in Tables 1, 2, 3, and 4. Polymerase chain reaction (PCR) products were sequenced using a Big Dye terminator cycle sequencing kit (version 3.1; Applied Biosystems) and an ABI 3130 automated sequencer (Applied Biosystems).

### Measurement of Serum Amino-Terminal proCNP Concentrations

Blood samples of III-1, II-5, I-2, and I-3 were centrifuged as soon as collected (15 min at 2,000×g, 4°C). The serum was stored

**Table 5.** Primer sets used for the analyses of transgenic mice.

| Name | Primer sequence (5′→3′) | | |
|---|---|---|---|
| | Forward | Reverse | Product size (bp) |
| SV40SD/SA -HA | CTAGGCCTGTACGGAAGTGTTAC | GTAATCTGGAACATCGTATGGGTA | 154 |
| Npr2–SV40 poly(A) | TGTGGAAATGAAGGGAAAAGG | TCACTGCATTCTAGTTGTGGTTTG | 149 |
| Sox9 | ACCCGCATCTGCACAACGCGGA | GGCTGGTACTTGTAATCGGG | 182 |
| Npr2 | TTTCCGGCCAAGCATT | GAGGTTGTCCAATATGCTGGT | 164 |
| Gapdh | CCCGTAGACAAAATGGTGAAG | ATGGCAACAATCTCCACTTTG | 104 |

SV40SD/SA-HA and Npr2-SV40 poly(A) were used to amplify the fragment derived from the transgene.

doi:10.1371/journal.pone.0042180.t005

at −80°C prior to use. NT-proCNP was assayed using an enzyme immunoassay (BIOMEDICA) according to the instructions provided. As a control, samples from 10 healthy adults (5 males and 5 females) were also measured.

## Construction of Expression Plasmids

The pcDNA3.1(+)/hemagglutinin (HA)-tagged human NPR2 wild-type vector (HA-WT) was a gift from Dr. Yoshihiro Ogawa (Tokyo Medical and Dental University, Japan) [21]. The construct encoding the mutant p.Val883Met, pcDNA3.1(+)/HA-human NPR2 Val883Met (HA-Val883Met), was generated by PCR-based mutagenesis using HA-WT as the template, and primers containing the nucleotide change. All the vector constructs were verified by bidirectional DNA sequencing.

## Cell Culture and Transfection

HEK293A cells were cultured in Dulbecco's modified Eagle's medium (DMEM) (Nacalai tesque) supplemented with 10% fetal bovine serum, 0.1 mM non-essential amino acid, and 2 mM L-glutamine at 37°C with 5% $CO_2$. HEK293A cells were plated at a density of $1\times10^5$ cells/12-well plate and cultured one day so as to reach confluence. Transfection was performed using the liposomal transfection reagent FuGENE6 (Reagent : DNA = 3 μl : 0.5 μg, Roche), according to the manufacturer's instructions. The cells were used for the experiments 48 hours (h) after transfection.

## Immunoblot Analysis

The transfected cells were scraped into lysis buffer, sonicated for 2–3 sec and centrifuged to harvest the supernatant as the whole-cell extract. Five micrograms of protein was fractionated on a 10% sodium dodecyl sulfate (SDS)-polyacrylamide gel and blotted to a nitrocellulose membrane. A mouse monoclonal antibody against HA-tag (6E2, 1:1000; Cell Signaling Technology) was used as the primary antibody. The signals were detected using SuperSignal West Dura Extended Duration Substrate (Thermo SCIENTIFIC) with a horseradish peroxidase-linked sheep anti-mouse IgG antibody (1:10,000; Promega). As an internal control, β-actin in each sample was detected with a monoclonal anti-β-actin antibody (1:4000; Sigma).

## Assay for cGMP of Transfected Cells and Plasma Samples

Transfected cells were serum-starved for 24 h before the cGMP assay and then incubated at 37°C with 5% $CO_2$ in DMEM containing 0.5 mM IBMX (3-isobutyl-1-methylxanthine) (Wako) for 10 min. The cells were next treated with $1\times10^{-8}$–$1\times10^{-6}$ M CNP-22 (Biochem) or vehicle (water) and incubated for another 10 min. The reaction was terminated with 300 μl of 0.1 M HCl, and the cGMP concentration was measured by a competitive enzyme immunoassay (Cayman Chemical). Results are presented as the mean ± SD. Student's *t* test was used for statistical analyses.

Plasma cGMP concentrations of III-1, II-5, I-2, I-3, and control samples were measured with a cyclic GMP radio immunoassay kit (YAMASA).

## Generation of the Transgenic Mice Expressing the p.Val883Met Mutant NPR2 in Chondrocytes

For the generation of transgenic mice expressing the mutant NPR2 (p.Val883Met) specifically in cartilage, we used the p742-Int vector (constructed by Tsumaki. et al.) [22], containing the promoter and intronic enhancer of the *Col11a2* gene. The cDNA encoding the mutant *Npr2* was obtained from pcDNA3.1(+)/HA-Val883Met, and inserted into the *Not I* site of p742-Int. The transgene was gel-purified and microinjected into the pronuclei of 250 fertilized eggs from C57BL/6 mice. For genotyping, genomic DNA from the tail was subjected to PCR.

The ethical treatment of animal protocol was approved by the Committee on the Ethics of Animal Experiments of the Osaka University Graduate School of Medicine (Permit Number J004081-003). All surgery was performed under isoflurane anesthesia, and all efforts were made to minimize suffering.

## Identification of Transgenic Founders

RNA samples were extracted from tail samples containing cartilage tissue. The end of the tail (10 mm) was cut off, immediately placed in RLT lysis buffer (QIAGEN), fractured by MicroSmash MS-100 (TOMY; 4800 rpm, 19 sec with ϕ5 mm zirconia-ball), and centrifuged at 15,000 rpm for 3 min. Total RNA was extracted from the supernatant using an RNeasy kit (QIAGEN). RNA was reverse-transcribed using the SuperScript III CellsDirect cDNA Synthesis System (Invitrogen). Real-time PCR was performed using SYBR® Green I fluorescence (Roche). Data were analyzed with LightCycler analysis software, version 3.5 (Roche). The amount of transgene mRNA was standardized based on that of murine *Sox9* mRNA, which is specifically expressed in chondrocytes. The transgene and murine *Sox9* primer sets for real-time PCR are listed in Table 5.

## Determination of the Npr2 mRNA Amount in Mouse Cartilage

RNA samples were isolated from the costal cartilage of line No.28 offspring (Tg. 28) and wild-type littermates (Wt) at postnatal day 5 under a stereomicroscope. For RNA extraction, the samples were treated as previously explained and real-time PCR was performed. The total amount of *Npr2* mRNA, which contains the sequence of mRNA from exon 15 to 16, and has complete commonality between humans and mice, was standardized based on that of murine *Gapdh* mRNA. The total *Npr2* and murine *Gapdh* primer sets for real-time PCR are listed in Table 5. Student's *t* test was used for statistical analyses.

## Assay for cGMP in Mouse Cartilage

The costal cartilage of Tg. 28 and Wt at postnatal day 5 was isolated under a stereomicroscope. The samples were immediately placed in 5% trichloroacetic acid (Wako), fractured by Micro-Smash MS-100 and centrifuged at 15,000 rpm for 3 min. The cGMP concentration was measured by a competitive enzyme immunoassay (Cayman Chemical) according to the manufacturer's directions. The pH of the cGMP standard and samples was neutralized with a phosphate buffer as previously described [23]. cGMP concentrations were standardized based on the DNA concentration of each sample, measured by an ultraviolet vision spectrophotometer for nucleic acid (NanoDrop 2000, Thermo SCIENTIFIC). Student's *t* test was used for statistical analyses.

## Soft X-ray Analysis of the Transgenic Mice

A soft X-ray analysis of the skeleton was performed using SOFTEX M-60 (30 kV, 3 mA, 80 sec, Softex), and faxitron X-ray (35 kV, 120 sec, Faxitron x-ray Corp).

## Histological Analysis

Femurs were harvested, fixed in 4% paraformaldehyde, and decalcified in EDTA solution. Sections were cut from paraffin-embedded specimens of knee-joint, and stained with hematoxylin-eosin (H&E).

## Acknowledgments

We thank Prof. Yoshihiro Ogawa for providing the expression vector for the human NPR2. We are grateful to Dr. Gen Nishimura for radiographic diagnosis.

## Author Contributions

Conceived and designed the experiments: KM NN MF YO HI T. Kitaoka T. Kubota HH CH NS NT HY TM KO. Performed the experiments: KM KO TM NN T. Kitaoka MF HI T. Kubota NT. Analyzed the data: KO NN MF YO HI T. Kitaoka NS. Contributed reagents/materials/analysis tools: KM NN MF YO HI T. Kitaoka T. Kubota HH CH NS NT HY TM KO. Wrote the paper: KM KO TM NN.

## References

1. Yasoda A, Ogawa Y, Suda M, Tamura N, Mori K, et al. (1998) Natriuretic peptide regulation of endochondral ossification. Evidence for possible roles of the C-type natriuretic peptide/guanylyl cyclase-B pathway. J Biol Chem 273: 11695–11700.
2. Teixeira CC, Agoston H, Beier F (2008) Nitric oxide, C-type natriuretic peptide and cGMP as regulators of endochondral ossification. Dev Biol 319: 171–178.
3. Schulz S (2005) C-type natriuretic peptide and guanylyl cyclase B receptor. Peptides 26: 1024–1034.
4. Potter LR, Abbey-Hosch S, Dickey DM (2006) Natriuretic peptides, their receptors, and cyclic guanosine monophosphate-dependent signaling functions. Endocr Rev 27: 47–72.
5. Chusho H, Tamura N, Ogawa Y, Yasoda A, Suda M, et al. (2001) Dwarfism and early death in mice lacking C-type natriuretic peptide. Proc Natl Acad Sci. U S A 98: 4016–4021.
6. Tsuji T, Kunieda T (2005) A loss-of-function mutation in natriuretic peptide receptor 2 (Npr2) gene is responsible for disproportionate dwarfism in cn/cn mouse. J Biol Chem 280: 14288–14292.
7. Tamura N, Doolittle LK, Hammer RE, Shelton JM, Richardson JA, et al. (2004) Critical roles of the guanylyl cyclase B receptor in endochondral ossification and development of female reproductive organs. Proc Natl Acad Sci U S A 101: 17300–17305.
8. Pejchalova K, Krejci P, Wilcox WR (2007) C-natriuretic peptide:an important regulator of cartilage. Mol Genet Metab 92: 210–221.
9. Bocciardi R, Giorda R, Buttgereit J, Gimelli S, Divizia MT, et al. (2007) Overexpression of C-type natriuretic peptide (CNP) is associated with overgrowth and bone anomalies in an individual with balanced t(2;7) translocation. Hum Mutat 28: 724–731.
10. Moncla A, Missirian C, Cacciagli P, Balzamo E, Legeai-Mallet L, et al. (2007) A cluster of translocation breakpoints in 2q37 is associated with overexpression of NPPC in patients with a similar overgrowth phenotype. Hum Mutat 28: 1183–1188.
11. Bartels CF, Bükülmez H, Padayatti P, Rhee DK, van Ravenswaaij-Arts C, et al. (2004) Mutations in the transmembrane natriuretic peptide receptor NPR-B impair skeletal growth and cause acromesomelic dysplasia, type Maroteaux. Am J Hum Genet 75: 27–34.
12. Matsukawa N, Grzesik WJ, Takahashi N, Pandey KN, Pang S, et al. (1999) The natriuretic peptide clearance receptor locally modulates the physiological effects of the natriuretic peptide system. Proc Natl Acad Sci U S A 96: 7403–7408.
13. Toydemir RM, Brassington AE, Bayrak-Toydemir P, Krakowiak PA, Jorde LB, et al. (2006) A novel mutation in FGFR3 causes camptodactyly, tall stature, and hearing loss (CATSHL) syndrome. Am. J Hum Genet 79: 935–941.
14. Yasoda A, Komatsu Y, Chusho H, Miyazawa T, Ozasa A, et al. (2004) Overexpression of CNP in chondrocytes rescues achondroplasia through a MAPK-dependent pathway. Nat Med 10: 80–86.
15. Zhang M, Su YQ, Sugiura K, Xia G Eppig JJ (2010) Granulosa cell ligand NPPC and its receptor NPR2 maintain meiotic arrest in mouse oocytes. Science 330: 366–369.
16. Tesmer JJ (2008) Guanylyl cyclase sees the light. J Biol 7: 31.
17. Lucas KA, Pitari GM, Kazerounian S, Ruiz-Stewart I, Park J, et al.(2000) Guanylyl cyclases and signaling by cyclic GMP. Pharmacol Rev 52: 375–414.
18. Wedel B, Garbers D (2001) The guanylyl cyclase family at Y2K. Annu Rev Physiol 63: 215–233.
19. Potter LR, Hunter T (2001) Guanylyl cyclase-linked natriuretic peptide receptors: structure and regulation. J Biol Chem 276: 6057–6060.
20. Mittendorf J, Weigand S, Alonso-Alija C, Bischoff E, Feurer A, et al. (2009) Discovery of riociguat (BAY 63–2521): a potent, oral stimulator of soluble guanylate cyclase for the treatment of pulmonary hypertension. Chem Med Chem 4: 853–858.
21. Hachiya R, Ohashi Y, Kamei Y, Suganami T, Mochizuki H, et al. (2007) Intact kinase homology domain of natriuretic peptide receptor-B is essential for skeletal development. J Clin Endocrinol Metab 92: 4009–4014.
22. Tsumaki N, Kimura T, Matsui Y, Nakata K, Ochi T (1996) Separable cis-regulatory elements that contribute to tissue- and site-specific alpha 2(XI) collagen gene expression in the embryonic mouse cartilage. J Cell Biol 134: 1573–1582.
23. Philippe P, Jacques G (1989) Enzyme immunoassays of adenosine cyclic 3′, 5′ - monophosphate and guanosine cyclic 3′, 5′ – monophosphate using acetylcholinesterase. Anal Chem 61: 447–453.

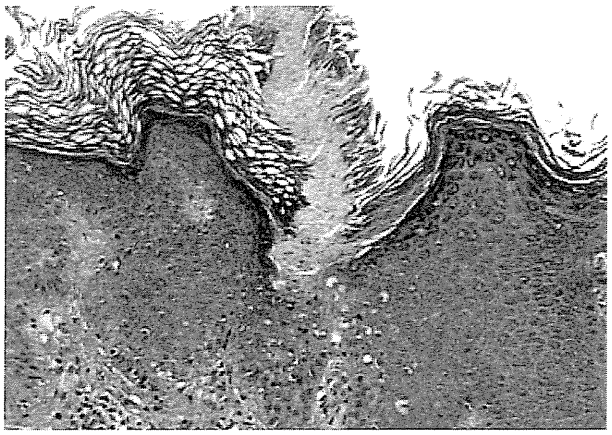

**Figure 2.** Photomicrograph of a skin lesion biopsy showing the typical histopathologic feature of porokeratosis (a column of parakeratosis overlying an invagination of the epidermis characterized by dyskeratotic keratinocytes: the "cornoid lamella") (hematoxylin and eosin, 10×).

3. Cha SH, Park HJ, Lee JY et al. Atypical porokeratosis developing following bone marrow transplantation in a patient with myelodisplastic syndrome. Ann Dermatol 2010;22:206–208.
4. Hong JB, Hsiao CH, Chu CY. Systematized linear porokeratosis: a rare variant of diffuse porokeratosis with good response to systemic acitretin. J Am Acad Dermatol 2009;60:713–715.
5. Marquez C, Bair SM, Smithberger E et al. Systemic retinoids for chemoprevention of non-melanoma skin cancer in high-risk patients. J Drugs Dermatol 2010; 9:753–758.

Riccardo G. Borroni, M.D., Ph.D.*
Dimitri Poddighe, M.D.†
Marco Zecca, M.D.‡
Valeria Brazzelli, M.D.¶
*Molecular Diagnostics Laboratory, †Pediatric Oncohematology, and ‡Institute of Dermatology, Fondazione IRCCS Policlinico San Matteo, Pavia, Italy
¶University of Pavia, Pavia, Italy

Address correspondence to Riccardo G. Borroni, M.D., Ph.D., Molecular Diagnostics Laboratory, Fondazione IRCCS Policlinico San Matteo, Viale C. Golgi 19, 27100 Pavia, Italy, or e-mail: r.borroni@smatteo.pv.it.

## Generalized Lichen Nitidus in Russell-Silver Syndrome

**Abstract:** **Generalized lichen nitidus is a rare disease, and there are only a few reports associating it with a genetic disorder. Here we report a case of generalized lichen nitidus in Russell-Silver syndrome.**

A 5-year-old Japanese girl presented with a 1-month history of papular eruption that gradually spread to her whole body. On examination, numerous small papules were seen on her trunk, head, and extremities. The individual papules were normal skin color, dome-shaped, 1 to 2 mm in size, with a glistening appearance, and with mild pruritus (Fig. 1A). The eruption seemed to spread to her whole body because of the Koebner phenomenon. Skin biopsy of the papule revealed an intense infiltration of lymphocytes and histiocytes into the papillary dermis immediately below the epidermis. The rete ridges at the margins of infiltration were elongated and encircled the infiltrated cells in a "ball-and-claw" manner. The overlying epidermis was thin and exhibited hyperkeratosis. The basal cell layer showed liquefaction degeneration (Fig. 1B). She was treated with a topical, compound of retinoic acid and tocopherol, which was selected because it had the effects of retinoic acid with rare irritation (1). Flattening of papules and remission of pruritus were observed after 6 months of application, but the lesions relapsed after discontinuation of the treatment. She continued without any medical treatment, and her lesions resolved spontaneously after 2 years.

The patient had intrauterine growth retardation (birth weight: 1,592 g at the gestational age of 38 wks) and postnatal growth retardation (height 1.37 standard deviations below the mean; weight 26.0% below the mean). She did not have any other endocrinological abnormalities that would cause growth retardation, such as hypothyroidism or growth hormone deficiency. She had the small triangular face, small narrow chin, down-turned corners of the mouth, and fifth-finger clinodactyly that are characteristics of Russell-Silver syndrome (RSS) (Fig. 1C).

From these clinical features, she was diagnosed with RSS, although she had neither maternal uniparental disomy of chromosome 7 nor hypomethylation of paternal imprinting center 1 of chromosome 11p15.5, which are reported in RSS (2).

Lichen nitidus is an uncommon, chronic papulosquamous condition of unknown etiology characterized by multiple shiny, dome-shaped papules. The majority of cases appear in children and young adults (2). The lesions are commonly localized and rarely generalized. Generalized lichen nitidus is sometimes reported in association with a genetic disorder such as Down syndrome, yet to our knowledge, this is a first report of generalized lichen nitidus in a patient with RSS (3,4).

RSS is a congenital disease mainly characterized by severe intrauterine growth retardation (94%) and postnatal growth retardation (99%). Other clinical features include a triangular-shaped face (79%), clinodactyly V (68%), and relative macrocephaly (64%) (2).

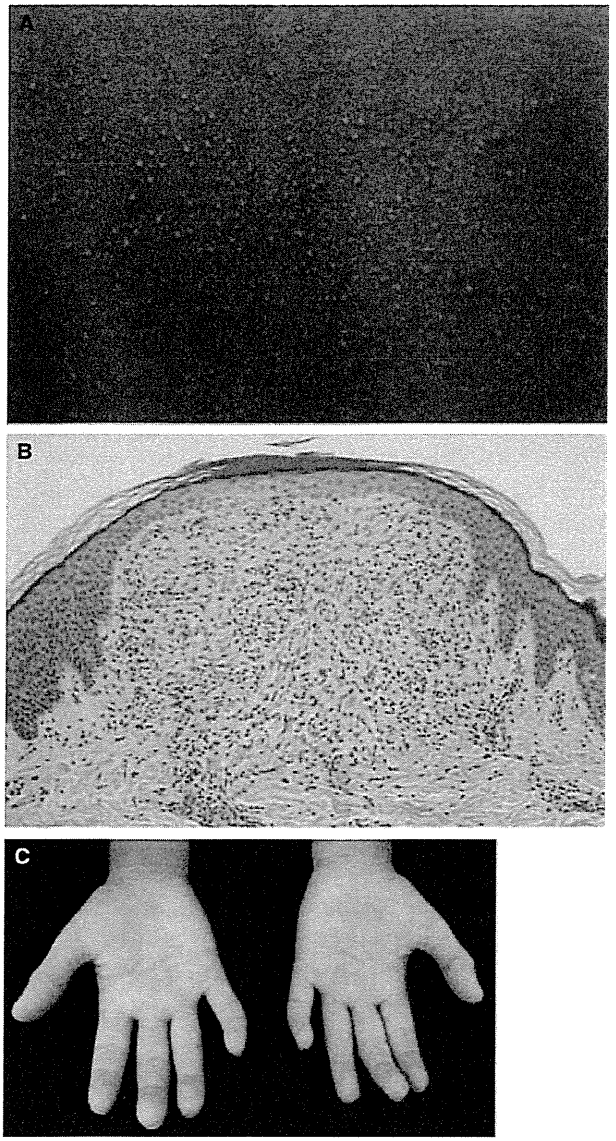


**Figure 1.** Clinical features and histological findings. (**A**) Shiny, dome-shaped, 1- to 2-mm papules on the patient's back due to Koebner phenomenon. (**B**) Well-circumscribed lymphocyte and histiocytes infiltration with elongated rete ridges at the margins of the infiltration. (**C**) Clinodactyly of the patient's fifth fingers.

RSS is classified as an imprinting disorder, and genetic and epigenetic disturbances are detected in approximately 50% of patients. Genetic disturbances include maternal uniparental disomy of chromosome 7 and hypomethylation in the imprinting control region 1 of 11p15.5 (2). Skin manifestations reported in RSS are hyperhidrosis and pigmentation disorders, including café au lait macules or diffuse brown pigmentation with a few small hypopigmented areas (5). Although imprinting disorders show many cutaneous features, it is not clear whether this case is an association between generalized lichen nitidus and RSS or a coincidental case. Further research and reports of similar cases are required to further explore this relationship.

## REFERENCES

1. Terao M, Nishida K, Murota H et al. Clinical effect of tocoretinate on lichen and macular amyloidosis. J Dermatol 2010;38:179–184.
2. Eggermann T. Russell-Silver syndrome. Am J Med Genet C Semin Med Genet 2010;154C:355–364.
3. Henry M, Metry DW. Generalized lichen nitidus, with perioral and perinasal accentuation, in association with Down syndrome. Pediatr Dermatol 2009;26:109–111.
4. Patrizi A, Di Lernia V, Pauluzzi P. [Generalized lichen niditus, trisomy 21 and congenital megacolon]. Ann Dermatol Venereol 1991;118:725.
5. Millington GW. Genomic imprinting and dermatological disease. Clin Exp Dermatol 2006;31:681–688.

Chie Kanai, M.D.*
Mika Terao, M.D., Ph.D.*
Atsushi Tanemura, M.D., Ph.D.*
Yoko Miyoshi, M.D., Ph.D.†
Keiichi Ozono, M.D., Ph.D.†
Ichiro Katayama, M.D., Ph.D.*
Departments of *Dermatology and †Pediatrics, Graduate School of Medicine, Osaka University, Osaka, Japan

Address correspondence to Mika Terao, M.D., Ph.D., 2-2 Yamadaoka, Suita, 565-0871, Osaka, Japan, or e-mail: mterao@derma.med.osaka-u.ac.jp.

# Extensive Facial and Orbital Infantile Hemangiomas Associated with High Intraocular Pressure

**Abstract:** **High intraocular pressure is a rare ophthalmic condition associated with infantile hemangiomas that involves the orbit, eyelid, or both. Here, we describe a patient with extensive facial and orbital infantile hemangiomas associated with high intraocular pressure in the affected eye. The prompt management of this challenging condition is essential.**

A 5-month-old, full-term girl presented with a small hemangioma on the right upper eyelid at birth that enlarged over the subsequent 4–6 weeks. [Correction added on 29 August 2012, after first online publication: the age of the patient was changed from '6-week-old' to '5-month-old'.] Extensive facial hemangiomas with numerous ulcerations (Fig. 1A) were observed upon

Cell Biology:

# FGF23 Suppresses Chondrocyte Proliferation in the Presence of Soluble α -Klotho both *in Vitro* and *in Vivo*

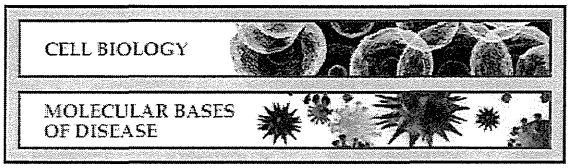


Masanobu Kawai, Saori Kinoshita, Akihito Kimoto, Yasuhiro Hasegawa, Kazuaki Miyagawa, Miwa Yamazaki, Yasuhisa Ohata, Keiichi Ozono and Toshimi Michigami

*J. Biol. Chem. 2013, 288:2414-2427.*
*doi: 10.1074/jbc.M112.410043 originally published online December 12, 2012*

---

THE JOURNAL OF BIOLOGICAL CHEMISTRY VOL. 288, NO. 4, pp. 2414–2427, January 25, 2013


# FGF23 Suppresses Chondrocyte Proliferation in the Presence of Soluble α-Klotho both *in Vitro* and *in Vivo*[*] [S]

Received for publication, August 16, 2012, and in revised form, December 3, 2012 Published, JBC Papers in Press, December 12, 2012, DOI 10.1074/jbc.M112.410043

**Masanobu Kawai[‡1], Saori Kinoshita[‡], Akihito Kimoto[§], Yasuhiro Hasegawa[¶], Kazuaki Miyagawa[‡], Miwa Yamazaki[‡], Yasuhisa Ohata[‡¶], Keiichi Ozono[¶], and Toshimi Michigami[‡]**

*From the Departments of [‡]Bone and Mineral Research and [§]Pathology, Osaka Medical Center and Research Institute for Maternal and Child Health, Izumi, Japan 594-1101 and the [¶]Department of Pediatrics, Osaka University Graduate School of Medicine, 565–0871 Suita, Japan*

**Background:** The role of elevated FGF23 in the development of growth retardation associated with X-linked hypophosphatemic rickets (XLH) remains elusive.
**Results:** FGF23 suppresses chondrocyte proliferation in cooperation with soluble α-Klotho.
**Conclusion:** Elevated FGF23 could have a causative role in the development of growth retardation in XLH.
**Significance:** This may provide insights into the unrecognized function of FGF23 signaling in chondrocyte biology.

**Fibroblast growth factor-23 (FGF23) is well established to play crucial roles in the regulation of phosphate homeostasis. X-linked hypophosphatemic rickets (XLH) is characterized by impaired mineralization and growth retardation associated with elevated circulating FGF23 levels. Administration of phosphate and calcitriol is effective in improving growth retardation, but is not sufficient to fully reverse impaired growth, suggesting the existence of a disease-specific mechanism in the development of growth retardation in addition to dysregulated phosphate metabolism. However, the precise mechanisms of growth retardation in XLH remain elusive. Here, we postulated that FGF23 suppressed chondrocyte proliferation in the presence of soluble α-Klotho (sKL). *In vitro* and *ex vivo* studies revealed that FGF23 formed a protein complex with sKL through KL1 internal repeat and suppressed the linear growth of metatarsals in the presence of sKL, which was antagonized by co-incubation with neutralizing antibodies against FGF23 or by knocking-down FGFR3 expression. Additionally, FGF23 binding to FGFR3 was enhanced in the presence of sKL. Histologically, the length of the proliferating zone was diminished and was associated with decreased chondrocyte proliferation. FGF23/sKL suppressed Indian hedgehog (Ihh) expression and administration of Ihh protein partially rescued the suppressive effect of FGF23/sKL on metatarsal growth. Intraperitoneal administration of sKL in *Hyp* mice, a murine model for XLH, caused a decrease in the length of the proliferating zone associated with decreased chondrocyte proliferation without altering circulating phosphate levels. These findings suggest that suppression of chondrocyte proliferation by FGF23 could have a causative role in the development of growth retardation in XLH.**

Emerging evidence from clinical and animal studies demonstrates pivotal roles of fibroblast growth factor 23 (FGF23)[2] signaling in the regulation of phosphate homeostasis (1–5). Osteoblast-lineage specific cells, especially osteocytes, produces large amounts of FGF23, but other tissues including small intestine, heart, and ventrolateral thalamic nucleus and thymus produce FGF23 as well although the physiological significance of FGF23 produced from these tissues remain to be defined (6, 7). FGF23 transduces its signals through its specific FGF receptors, which requires α-Klotho, a 130-kDa single-pass transmembrane protein, as a co-receptor (8, 9). Contrary to a widely accepted tenet that membrane-bound α-Klotho is mandatory for FGF23 to activate its downstream signaling pathways in physiological conditions (7, 8), accumulating evidence highlights the possibility that FGF23 may stimulate its downstream signaling pathways in cells that lack or have little expression of membrane-bound α-Klotho. Although membrane-bound α-Klotho is not expressed in the skeleton, FGF23 may be operative in skeletal cells (10, 11). Sitara *et al.* generated a mouse model where both *Fgf23* and *Slc34a1*, encoding for the type IIa sodium-phosphate ($Na^+$/Pi) co-transporter, were deleted to reverse the hyperphosphatemia noted in *Fgf23*-null mice (10). These double mutants exhibited similar skeletal phenotypes to *Fgf23*-null mice, despite a correction in serum phosphate levels, suggesting the possibility of a phosphate-independent action of FGF23 in the skeleton. In the same vein, adenoviral transduction of FGF23 in rat calvarial osteoblasts has been shown to stimulate osteoblastogenesis and mineralization (11). In addition, there is mounting evidence that soluble α-Klotho (sKL) has been implicated to have biological functions in experimental models. For example, sKL has been shown to inhibit insulin and IGF-I signaling (12). Another levels of examples include the antagonistic effects of sKL on Wnt signaling and TGF-β signaling pathways (13, 14). Of note is that sKL has also been implicated to mediate FGF23 signaling in cells which do not express membrane-bound α-Klotho (15). Combined together, these lines of evi-

* This work was supported in part by a grant from the Japan Foundation for Pediatric Research (to M. K.).
[S] This article contains supplemental Figs. S1–S4.
[1] To whom correspondence should be addressed: Department of Bone and Mineral Research, Osaka Medical Center and Research Institute for Maternal and Child Health, 840 Murodo-cho Izumi, Osaka, 594-1101, Japan. Tel.: 81-725-56-1220; Fax: 81-725-57-3021; E-mail: kawaim@mch.pref.osaka.jp.

[2] The abbreviations used are: FGF, fibroblast growth factor; XLH, X-linked hypophosphatemic rickets; sKL, soluble α-Klotho; Ihh, Indian hedgehog.

dence indicate that FGF23 may have a non-canonical function such that FGF23 can exert its signals in cells that do not express functional membrane-bound α-Klotho such as chondrocytes, which may be more relevant in the presence of sKL.

Growth retardation is mainly caused by a defect in chondrogenesis and is one of the significant complications in children suffering from a disorder with dysregulated phosphate and vitamin D metabolism. X-linked hypophosphatemic rickets (XLH) is a disorder with a loss-of-functional mutation in the *PHEX* gene (16). These patients exhibit elevated serum FGF23 levels associated with decreased serum phosphate and 1,25-dihydroxyvitamin D levels. The skeletal phenotype of these patients includes growth retardation as well as rickets and impaired mineralization. Administration of phosphate and calcitriol is effective in improving rickets and growth retardation, but it is well recognized that impaired linear growth still remains despite the correction in biochemical markers and rachitic changes (17). Abnormal phosphate and vitamin D metabolism is likely to be the leading cause of growth retardation associated with XLH, but the fact that normalization of dysregulated phosphate and vitamin D levels did not fully reverse impaired growth led us to speculate that there could be a disease-specific mechanism that modulates the development of growth retardation in addition to dysregulated phosphate and vitamin D metabolism. Interestingly, Liu *et al.* showed that shortening of the tibia in *Hyp* mice, a murine model for XLH carrying a 3′-deletion in the *Phex* gene, was partially rescued by crossing these mice with *Fgfr3* deficient mice without altering circulating phosphate and vitamin D levels, indicating that signals exerted from FGFR3 may be partly responsible for the development of growth retardation in *Hyp* mice (18). These lines of evidence prompted us to hypothesize that elevated FGF23 levels may be at least in part responsible for the development of growth retardation in XLH patients through activating FGF receptors in chondrogenic cells.

## EXPERIMENTAL PROCEDURES

*Mice*—C57BL/6J mice were purchased from CLEA Japan, Inc. and *Hyp* mice on a C57BL/6J background were kindly provided by Dr. T. Tanaka (Okayama University Graduate School of Medicine). Mice were maintained with free access to water and standard chow (CE-2, CLEA Japan, Inc) on a 12:12 h LD cycle in a pathogen-free animal facility. All animal studies were reviewed and approved by the Institutional Animal Care and Use Committee of Osaka Medical Center and Research Institute for Maternal and Child Health.

*Reagents and Cell Lines*—Recombinant human FGF23 and neutralizing antibody against FGF23 were kindly provided by Kyowa Hakko Kirin Co., Ltd. Mouse anti-Klotho antibody (Mink1) was a kind gift from Drs. A. Imura and Y. Nabeshima (Institute of Biomedical Research and Innovation). Recombinant mouse soluble α-Klotho and rat anti-Klotho antibody (AF1819) were purchased from R&D Systems. Rat anti-Klotho antibody (Clone KM2076, KO603) was obtained from TransGenic Inc. Expression vector containing human FGFR3 (pcDNA3-hFGFR3) was kindly provided from Dr. K. Hasegawa (Okayama University Graduate School of Medicine). ATDC5 cells were obtained from the Human Science Research Resources Bank (Osaka, Japan) and maintained in DMEM/F12 medium supplemented with 5% fetal bovine serum and 1% insulin-transferrin-selenium-G supplement. For chondrogenic induction, cells were incubated with alpha minimal essential medium (αMEM) supplemented with 5% FBS and ITS.

*Isolation of Primary Chondrocytes*—Primary chondrocytes were isolated from rib cages obtained from 3-day old C57BL6/J mice as previously described (19). Briefly, cartilage was incubated with actinase E (2 mg/ml in PBS, Kaken Pharmaceutical Co. Ltd., Tokyo, Japan) for 30 min at 37 °C, followed by digestion with collagenase (3 mg/ml, Wako) for 90 min at 37 °C. Pellets collected by the centrifuge were washed, passed through a 100-μm cell strainer, and used as primary chondrocytes. Primary chondrocytes were cultured in DMEM supplemented with 10% FBS and 50 μg/ml of ascorbic acid.

*Generation of Truncated sKL Mutant*—Truncated mutants containing KL1 internal repeat (sKL-KL1: aa1–536) or KL2 internal repeat (sKL-KL2: aa537–958) were created by subcloning the corresponding PCR products into pENTR vector using pENTR Directional TOPO cloning kit (Invitrogen) and transferred to pcDNA3.2/V5 vectors using LR recombination reaction system (Invitrogen).

*Metatarsal Organ Culture*—Middle metatarsals were isolated from E15.5 C57BL/6J mouse embryos and incubated in αMEM containing 0.5% BSA, 50 μg/ml ascorbic acid, and 1 mM β-glycerol phosphate as previously described (20). Stimulants were added to culture media on day 0, day 1, and every other day from day 1 for indicated periods. For BrdU labeling, metatarsals were incubated with BrdU for 3 h according to the manufacturer's instructions (Calbiochem). To visualize calcium deposition, metatarsals were labeled with calcein (500 ng/ml) for 2 h. Bones were then fixed with 4% PFA, embedded in paraffin, and processed for hematoxylin and eosin staining and immunohistochemistry.

*Western Blot Analysis*—To prepare whole cell lysates, cells were solubilized in RIPA buffer (1% Triton, 1% Na deoxycholate, 0.1% SDS, 150 mM NaCl, 10 mM Tris-Cl (pH 7.4), 5 mM EDTA, 1 mM orthovanadate, and protease inhibitor mixture (Complete TM; Roche). Equal amounts of protein were separated by SDS-PAGE and transferred electrophoretically to PVDF membranes. Membranes were blocked in BlockAce reagent (Dainippon Pharmaceuticals, Osaka, Japan) or Blocking-one P reagent (Nacalai Tesque), immunoblotted with anti-ERK (1:1000, 9102, Cell Signaling), anti-pERK (1:1000, 9101, Cell Signaling), anti-FRS2α (1:1000, sc-8318, Santa Cruz Biotechnology), anti-pFRS2α (1:1000, 3864, Cell Signaling), or anti-GAPDH (1:2000, sc-20357, Santa Cruz Biotechnology) and developed with horseradish peroxidase-coupled secondary antibodies, followed by enhancement with a chemiluminescence (ECL) detection system (GE Healthcare).

*Co-immunoprecipitation*—Cells were solubilized in IP buffer (5 mM EDTA, 150 mM NaCl, 0.5% Nonidet P-40, 10% glycerol, and 10 mM Tris-HCl, pH 8.0) containing a protease inhibitor mixture (Complete TM, EDTA-free; Roche Diagnostics) and centrifuged. Supernatants were incubated with antibody, followed by immunoprecipitation with protein A/G-Sepharose (Santa Cruz Biotechnology) at 4 °C overnight. Where conditioned media were used for co-immunoprecipitation, condi-

tioned media obtained from either CHO cells stably expressing FGF23R179Q which is a proteolysis-resistant mutant or HEK293 cells stably expressing soluble α-Klotho were mixed and incubated with antibody, followed by immunoprecipitation with protein A/G-Sepharose (Santa Cruz Biotechnology) at 4 °C overnight. Samples were washed five times with IP buffer and then subjected to Western blot analysis.

*Immunohistochemistry*—Samples were fixed in 10% buffered formalin and immunohistochemical analysis was performed using paraffin-embedded samples. Femurs were decalcified using 20% EDTA solution for 7 days before paraffin-embedding. After deparaffinization and rehydration, antigen retrieval was performed using citrate buffer at 95 °C for 60 min (for Sox9 and Ihh), pepsin solution (Cat AP-9007-005, Thermo Scientific) at 37 °C for 10 min (for Col2a1) or proteinase K solution (0.4 mg/ml, Cat S3020, DAKO) at room temperature for 5 min (for Fgfr3). Endogenous peroxidase activity was quenched using ImmunoCruz staining systems (Santa Cruz Biotechnology). Following blocking, sections were incubated with anti-Sox9 antibody (1:100; sc-20095, Santa Cruz Biotechnology), anti-Ihh antibody (1:50; sc-1196 Santa Cruz Biotechnology), anti-Col II mouse monoclonal antibody (Clone 2B1.5, MS-235-R7, Thermo Fisher Scientific, Waltham, MA), anti-Fgfr3 antibody (1:100, SAB4500888, Sigma) overnight at 4 °C. Normal IgG was used as a negative control. Sections were then incubated with a biotinylated secondary antibody, followed by incubation with streptavidin-biotinylated HRP complex, and visualized with 3, 3′-diaminobenzidine using ImmunoCruz Staining Systems (Santa Cruz Biotechnology). The TUNEL assay was performed using the *In situ* Apoptosis Detection kit (Takara Bio Inc.) according to the manufacturer's protocol.

*In Situ Hybridization*—Digoxigenin-labeled riboprobes were synthesized by an *in vitro* transcription reaction using a DIG RNA labeling kit according to manufacturer's protocol (Roche Applied Science). Paraffin-embedded sections were deparaffinized, rehydrated, and incubated with proteinase K solution. Sections were then fixed with PFA, treated with 0.25% acetic acid, and incubated with a prehybridization buffer, followed by hybridization with digoxigenin-labeled riboprobes. After hybridization, sections were incubated with anti-DIG-alkaline phosphatase-conjugated antibody and visualized by 4-nitro blue tetrazolium chloride and 5-bromo-4-chloro-3-indolyl-phosphate.

*Adenovirus-mediated Knock-down Experiments*—Knock-down of Fgfr3 expression in metatarsals was performed based on adenovirus-mediated expression of the microRNA (miRNA) system using the BLOCK-iT™ Pol II miR RNAi Expression Vector Kit with EmGFP (Invitrogen). Recombinant adenoviruses were prepared using the ViraPower™ Adenovirus Expression System (Invitrogen) according to the manufacturer's protocol. Each metatarsal was infected with $1 \times 10^7$ particles of adenovirus in the presence of poly-L-lysine for 4 h on day 0, 1, and every other day from day 1.

*In Vitro and ex Vivo Treatment with FGF23 and/or sKL*—Where FGF23 and sKL combinational treatment was used, FGF23 and sKL were mixed and pre-incubated for 5 min at room temperature before adding to culture media.

*In Vivo sKL Administration*—From postnatal day 7, 0.02 mg/kg of sKL was intraperitoneally administered in wild-type or *Hyp* mice for 3 days.

*In Vivo BrdU Assay*—BrdU (100 μg/gBW) and FdU (12 μg/gBW) were injected intraperitoneally as described previously (20). Two hours after injection, tibiae were collected and fixed in 4% PFA overnight at 4 °C. Tibiae were decalcified using 20% EDTA (pH 7.4) for 14 days and subjected to immunohistochemistry for BrdU. Following this, blocking sections were incubated with a mouse monoclonal anti-BrdU antibody (1:100, Calbiochem) overnight at 4 °C. Sections were then incubated with a biotinylated goat anti-mouse secondary antibody, followed by incubation with streptavidin-biotinylated HRP complex, and visualized with 3,3′-diaminobenzidine.

*Generation of Conditioned Media*—The expression vector containing Indian hedgehog (pcDNA3.1-Ihh) was kindly provided by Dr. Nishimura (Osaka University School of Dentistry). pcDNA3.1-Ihh or an empty vector was transfected into HEK293 cells using FuGene HD reagent (Promega) in DMEM containing 10% fetal calf serum. Two days post-transfection; conditioned media were collected and centrifuged to remove cell debris.

*Measurement of Serum Parameters*—Measurement of plasma phosphate and FGF23 concentrations was carried out using P-test Wako (Wako) and sandwich ELISA (Kainos Laboratory), respectively, following manufacturers' instructions.

*Statistical Analysis*—All data are expressed as the mean ± S.E. Results were analyzed for significant differences using the Student's *t* test or ANOVA followed by the Bonferroni multiple comparison *post hoc* test. Significance was set at $p < 0.05$.

## RESULTS

*FGF23 Elicits Its Signals in the Presence of Soluble α-Klotho in Chondrocytes in Vitro*—To investigate whether FGF23 exerts direct effects on chondrocytes, we examined the expression profile of α-Klotho in chondrogenic ATDC5 cells and primary chondrocytes since α-Klotho has been shown to be required for FGF23 to mediate its signals. *α-Klotho* transcripts were detectable in these cells by real-time RT-PCR, but expression levels were more than hundred times lower than those in the anterior pituitary, known to abundantly express *α-Klotho* (supplemental Fig. S1*A*). Consistent with the extremely low levels of *α-Klotho* transcripts in chondrogenic cells, immunohistochemical analysis failed to detect α-Klotho protein expression in metatarsals (supplemental Fig. S1*B*). In addition, the expression profile of *α-Klotho* did not show any alteration during *in vitro* chondrogenesis (supplemental Fig. S1*A*). These lines of evidence led us to speculate that α-Klotho is unlikely to be functional in chondrogenic cells. Consistent with this speculation, recombinant FGF23 protein failed to induce ERK1/2 phosphorylation in chondrogenic cells, although FRS2α was weakly phosphorylated by FGF23 at a dose of 100 ng/ml (Fig. 1, *A* and *C*). These data indicate that FGF23 alone is not likely to exert its action on chondrogenic cells due to the lack of functional α-Klotho expression. Because there is evidence that sKL has an important role in mediating FGF23 signaling pathways in cells that do not express functional α-Klotho, we tested the concept that FGF23 may elicit its signals in the presence of sKL

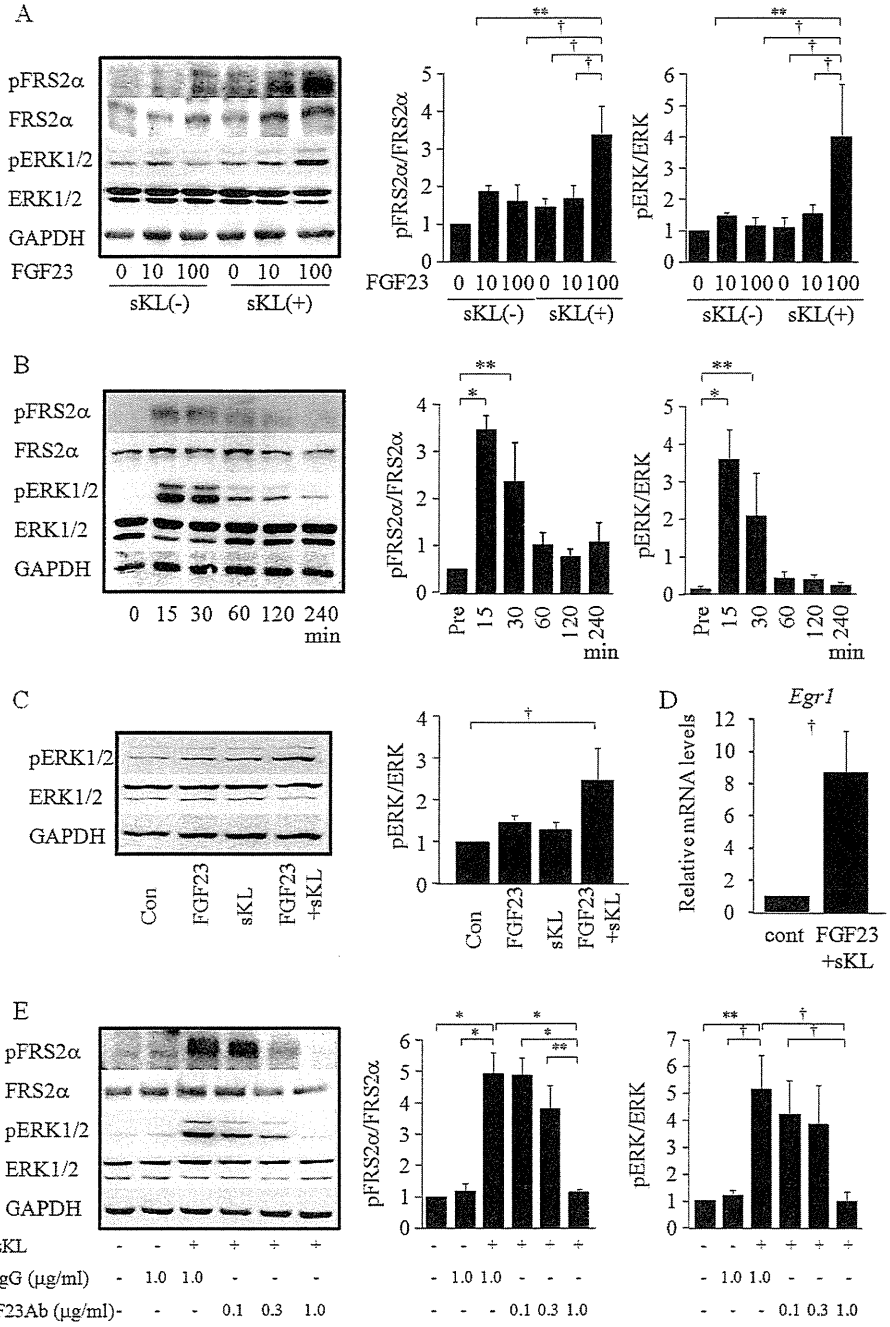


FIGURE 1. **FGF23 activates downstream signaling pathways in the presence of sKL in chondrogenic cells.** *A–C*, ATDC5 cells were treated with FGF23 in the presence or absence of sKL (100 ng/ml) for 15 min (*A*) or FGF23 (100 ng/ml) and sKL (100 ng/ml) for the indicated period (*B*). Primary chondrocytes were treated with FGF23 (100 ng/ml), sKL (100 ng/ml), or both for 15 min (*C*). Western blot analysis was performed using whole cell lysates and quantification was performed using densitometry ($n = 3$–4). *D*, ATDC5 cells were treated with FGF23 (100 ng/ml) and sKL (100 ng/ml) for one hour. Expression of *Egr1* was determined by real-time RT-PCR ($n = 3$). *E*, ATDC5 cells were treated with FGF23 (100 ng/ml) and sKL (100 ng/ml) in the presence or absence of neutralizing antibodies for FGF23 (anti-FGF23 Ab) at the indicated concentration for 15 min. Normal mouse IgG was used as a control for anti-FGF23 Ab. Western blot analysis was performed using whole cell lysates and quantification was performed using densitometry ($n = 3$). The figures shown are the representative from at least three independent experiments. The values were expressed as mean ± S.E. *, $p < 0.001$; **, $p < 0.01$; †, $p < 0.05$.

in chondrogenic cells. First, we analyzed whether FGF23 can form a protein complex with sKL. Co-immunoprecipitation analysis using HEK293 cells over-expressing FGF23 and/or sKL revealed that FGF23 can form a protein complex with sKL in these cells (Fig. 2*A*). Because both sKL and FGF23 are secretory molecules, we next performed co-immunoprecipitation analysis using the conditioned media containing FGF23 or sKL, or solutions of recombinant FGF23 and/or sKL proteins and found that FGF23 and sKL can make a protein complex in a solution as well (Fig. 2, *B* and *C*). To determine the responsible domain of this interaction, we generated truncated mutants containing either KL1 internal repeat or KL2 internal repeat and found that KL1 internal repeat was involved in the interaction between sKL and FGF23 (Fig. 2*D*). Based on these observations, we next examined the effect of sKL with respect to FGF23 signaling in chondrogenic cells. FGF23 in the presence

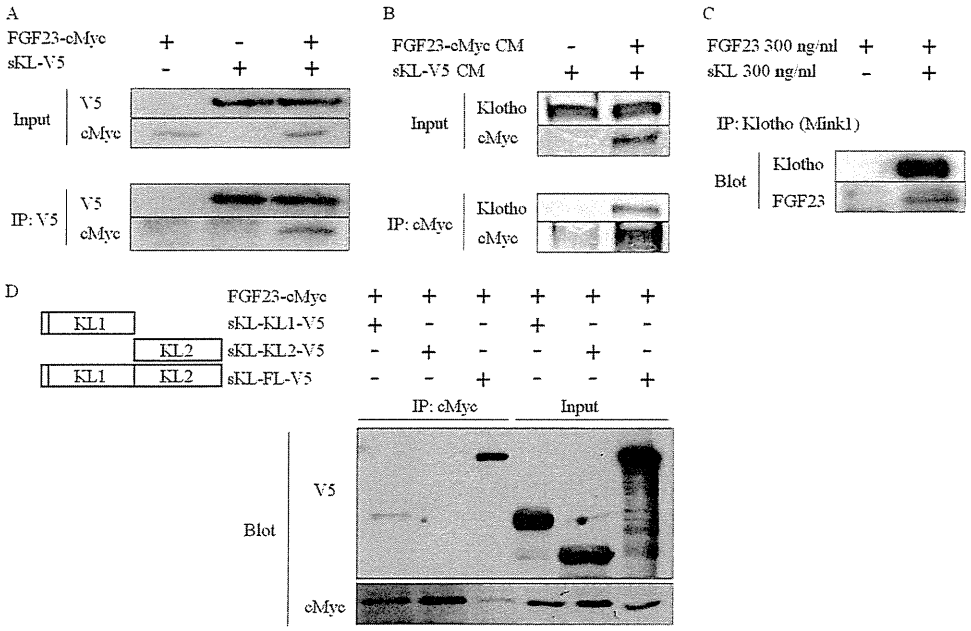


FIGURE 2. **FGF23 makes a protein complex with sKL.** *A*, HEK293 cells were transfected with FGF23-cMyc or sKL-V5 expression vectors. Immunoprecipitation with V5 was followed by Western blot analysis for cMyc. *B*, conditioned-media containing FGF23-cMyc were mixed with sKL-containing conditioned-media. Immunoprecipitation with cMyc was followed by Western blot analysis for Klotho (AF1819). *C*, 300 ng of recombinant FGF23 and recombinant sKL were mixed in one milliliter solution and immunoprecipitation with Klotho (Mink1) was followed by Western blot analysis for Klotho (KM2076). *D*, HEK293 cells were transfected with FGF23-cMyc, and full-length (sKL-FL-V5) or truncated sKL (sKL-KL1-V5 or sKL-KL2-V5) expression vectors. Immunoprecipitation with cMyc was followed by Western blot analysis for V5. The figures shown are the representative from at least three independent experiments.

of sKL (FGF23/sKL) induced FRS2$\alpha$ and ERK1/2 phosphorylation both in ATDC5 and primary chondrocytes in a dose- and time-dependent manner, although sKL alone did not show any effect on phosphorylation of these proteins (Fig. 1, *A--C*). In addition, FGF23/sKL induced the expression of *Early growth response 1* (*Egr1*), a target gene of FGF23 signaling, in ATDC5 cells (Fig. 1*D*). Importantly, phosphorylation of FRS2$\alpha$ and ERK1/2 by FGF23/sKL was completely blocked by co-incubation with neutralizing antibodies raised against FGF23 (anti-FGF23 Ab), confirming the specificity of FGF23 in activating FRS2$\alpha$ and ERK1/2 signaling in chondrogenic cells (Fig. 1*E*).

*FGF23 Impairs Linear Growth of Metatarsals in the Presence of sKL ex Vivo*—To better understand the role of FGF23/sKL signaling in chondrocyte biology, we introduced an *ex vivo* metatarsal organ culture system to analyze the effect of FGF23/sKL on metatarsal growth. Neither FGF23 alone nor sKL alone exhibited any effects on the linear growth of metatarsals, but when metatarsals were treated with FGF23 in the presence of sKL, their linear growth was significantly impaired in a dose-dependent manner (Fig. 3, *A--D*). To confirm the specificity of FGF23 signaling in the suppression of metatarsal growth, we treated metatarsals with FGF23/sKL in the presence or absence of anti-FGF23 Ab. Although treatment with anti-FGF23 Ab alone did not affect the linear growth of metatarsals compared with control-IgG treatment (supplemental Fig. S2), the inhibitory effect of FGF23/sKL on metatarsal linear growth was completely abolished by co-incubation with anti-FGF23 Ab (Fig. 3, *E* and *F*).

*FGF Receptor 3 Mediates the Suppressive Effect of FGF23/sKL on Metatarsal Linear Growth*—Next, we examined whether FGF receptor 3 (FGFR3) is involved in the suppressive effect of FGF23/sKL on metatarsal growth. We first investigated expression levels of FGFR3 in metatarsals treated with FGF23/sKL and found that expression and localization of FGFR3 was comparable between metatarsals treated with or without FGF23/sKL (Fig. 4, *A* and *B*). Second, we suppressed FGFR3 expression in metatarsals using adenovirus-mediated transduction of microRNA specific for *Fgfr3* and examined the effect of FGF23/sKL on metatarsal growth. Transduction of adenovirus in metatarsals was determined by visualizing the fluorescence of EmGFP (Fig. 4, *C* and *D*), and immunohistochemistry and real-time PCR analyses for FGFR3 confirmed the efficient knock-down of FGFR3 in metatarsals (Fig. 4, *E* and *F*). As shown in Fig. 4*G*, FGF23/sKL showed an inhibitory effect on linear growth in metatarsals infected with control-miRNA, whereas the suppressive effect of FGF23/sKL on metatarsal growth was partly abolished in metatarsals infected with miRNA specific for *Fgfr3*. These findings imply that the effect of FGF23/sKL is at least in part mediated through FGFR3 in metatarsals.

*Physical Interaction between FGF23 and FGFR3 Is Enhanced in the Presence of sKL*—We next investigated the mechanism whereby sKL enhanced FGF23 signaling. Because FGFR3 is involved in the suppressive effect of FGF23/sKL on metatarsal growth, we assessed whether the binding of sKL or FGF23 to FGFR3 was affected by FGF23 or sKL, respectively. Co-immunoprecipitation analysis revealed that the interaction of sKL with FGFR3 was augmented in the presence of FGF23 (Fig. 5*A*). In addition, binding of FGF23 to FGFR3 was enhanced as well when sKL was present (Fig. 5*B*). These data indicate that one of the mechanisms by which sKL enhanced FGF23 signaling pathway would be mediated through enhancing the accessibility of FGF23 to its receptors.

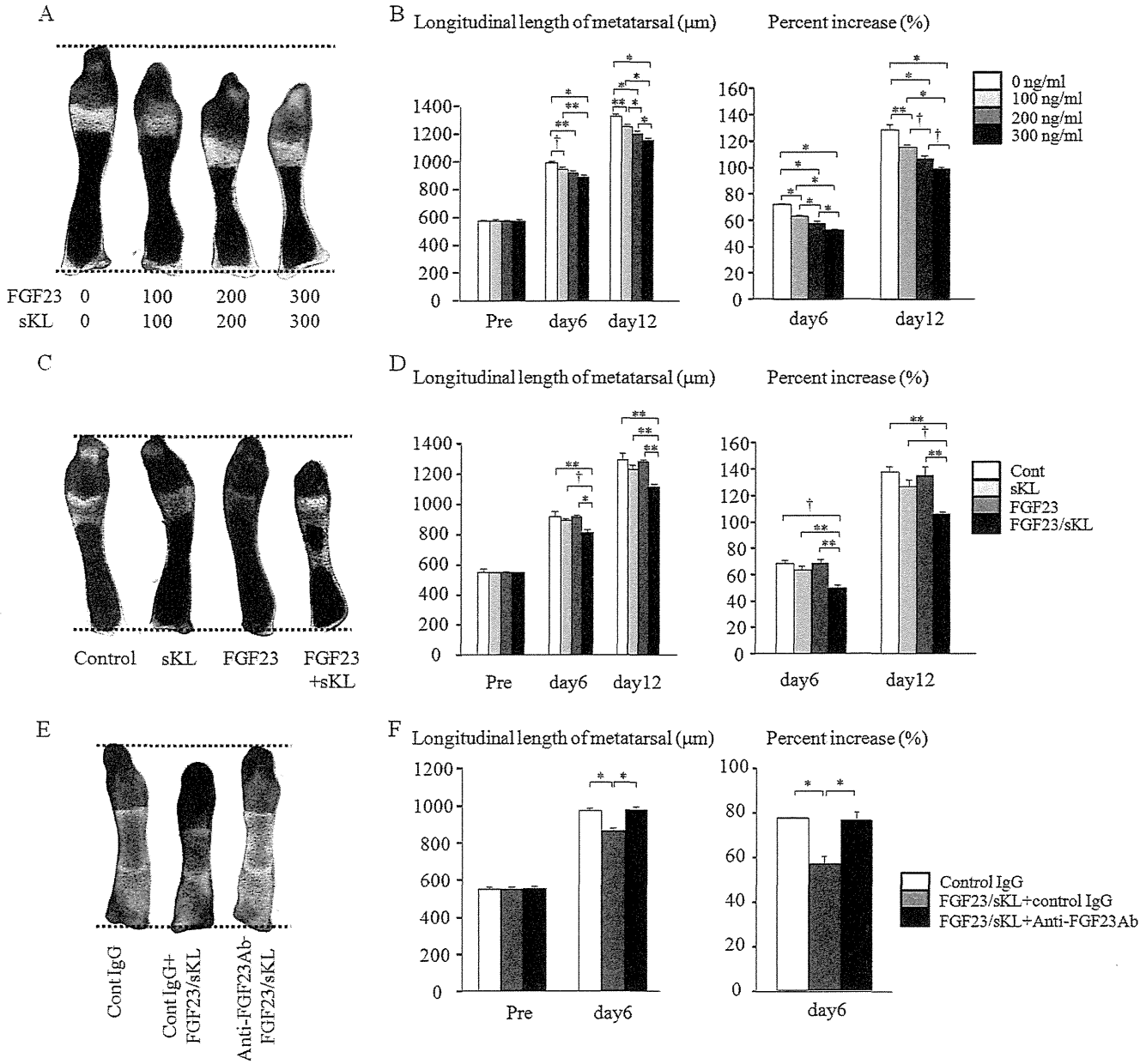


FIGURE 3. **FGF23 impairs longitudinal growth of metatarsals in cooperation with sKL.** *A–D*, metatarsals were cultured for 12 days in various concentrations of FGF23 and sKL as indicated (*A* and *B*) or treated with FGF23 (300 ng/ml), sKL (300 ng/ml), or both (*C* and *D*). Longitudinal lengths and percent increases in metatarsals were measured ($n = 3–4$). *E* and *F*, metatarsals were cultured with FGF23 (300 ng/ml) and sKL (300 ng/ml) in the presence or absence of neutralizing antibodies for FGF23 (anti-FGF23 Ab) (3 μg/ml) for 6 days, and longitudinal lengths and percent increases in metatarsals were measured ($n = 3–4$). Normal mouse IgG was used as a control for anti-FGF23 Ab. The values were expressed as mean ± S.E. *, $p < 0.001$; **, $p < 0.01$; †, $p < 0.05$.

*FGF23/sKL Impairs Chondrocyte Proliferation and Maturation*—To elucidate the mechanisms by which FGF23/sKL impairs metatarsal growth, we performed histological analyses and found that the length of the proliferating zone was decreased in metatarsals treated with FGF23/sKL, whereas the length of the resting zone was longer in FGF23/sKL-treated metatarsals than that in controls, but the difference did not reach significance (Fig. 6, *A* and *B*). These findings raised the possibility that FGF23/sKL possessed a context-specific effect on chondrocyte proliferation where FGF23/sKL inhibited chondrocyte proliferation in the proliferating zone. To prove this possibility, we performed BrdU labeling of these metatarsals to determine chondrocyte proliferation. As shown in Fig. 6, *C* and *D*, the BrdU index was significantly lower in the proliferative zone of FGF23/sKL-treated metatarsals than that in controls, whereas the BrdU index was enhanced in the resting zone of FGF23/sKL-treated metatarsals. Because there is a possibility of the involvement of cell apoptosis for the decreased length of proliferating zone, we also analyzed whether cell apoptosis was enhanced by the treatment with FGF23/sKL. TUNEL assay revealed that cell apoptosis of proliferating chondrocyte was not different between metatarsals treated with or without FGF23/sKL (Fig. 6*E*). To further understand the mechanisms of decreased chondrocyte proliferation in the proliferating zone, we analyzed expression levels of *Sox9*, a master transcription factor for chondrocyte differentiation, and one of its target

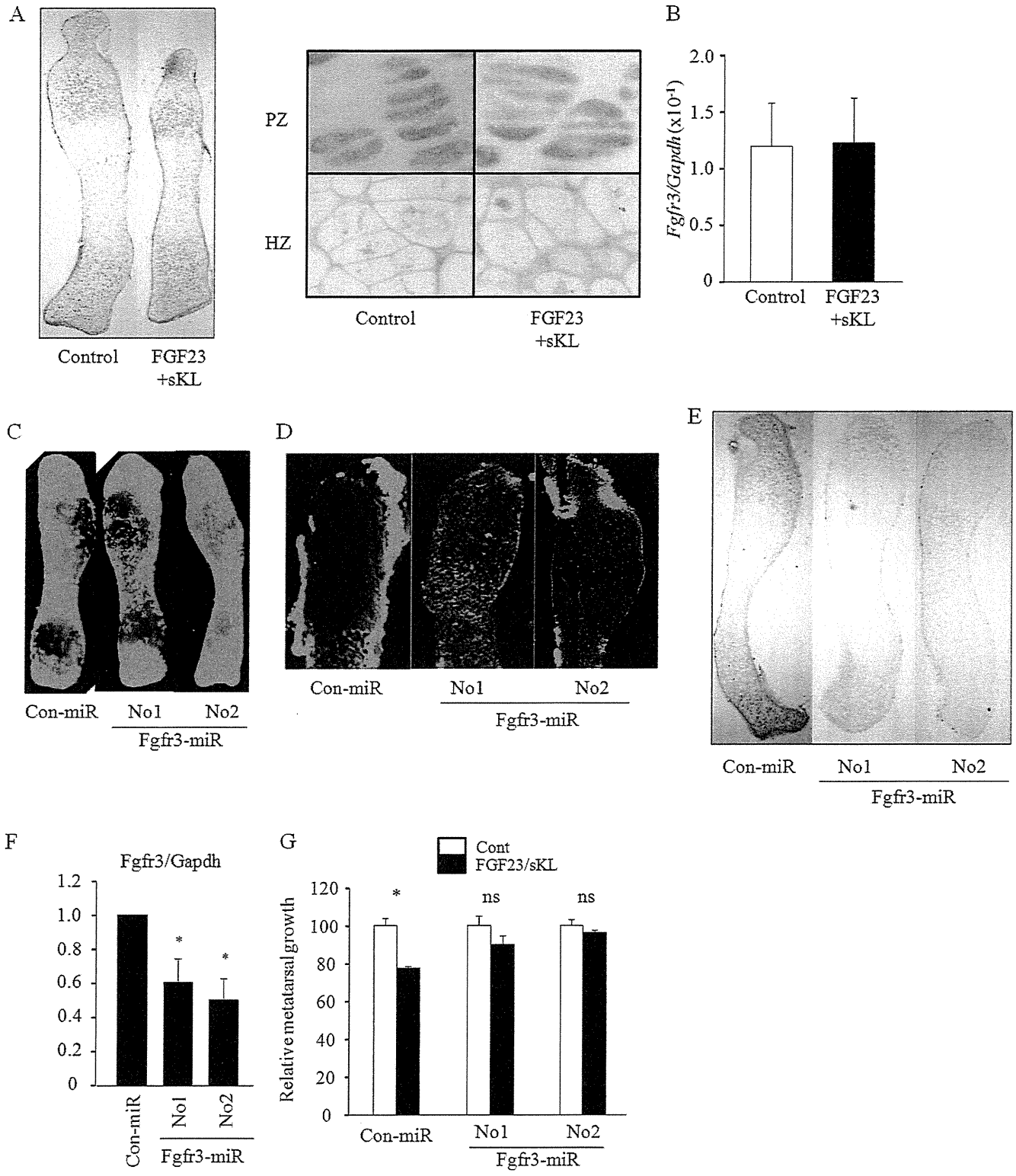


FIGURE 4. **FGFR3 partly mediates the suppressive effect of FGF23/sKL on metatarsal growth.** *A* and *B*, metatarsals were cultured in the presence or absence of FGF23 (300 ng/ml) and sKL (300 ng/ml) for 6 days. FGFR3 expression was analyzed by immunohistochemistry (*A*) and real-time RT-PCR (*B*) ($n = 3$). *C–F*, metatarsal rudiments were infected with adenovirus harboring control miRNA (con-miR) or *Fgfr3*-specific miRNA (Fgfr3-miR) for 6 days. Fluorescence of EmGFP was detected in metatarsals(*C*). Frozen metatarsals were sectioned and transduction of adenovirus was visualized by detecting the fluorescence of EmGFP (*D*). FGFR3 expression was analyzed by immunohistochemistry (*E*) and real-time RT-PCR (*F*) ($n = 3$). *G*, metatarsals infected with adenovirus containing either con-miR or Fgfr3-miR were cultured in the presence or absence of FGF23 (300 ng/ml) and sKL (300 ng/ml) for 6 days. Relative percent increases in longitudinal metatarsal growth were calculated ($n = 3–6$). The figures shown are the representative from at least three independent experiments. The values were expressed as mean ± S.E. *, $p < 0.05$. *ns*, not significant.

genes, *Col2a1*, to determine whether transcriptional machinery of chondrogenesis is affected by FGF23/sKL treatment. Chondrogenesis of primary chondrocytes analyzed by Alcian blue staining was not affected by FGF23/sKL treatment (Fig. 7*A*), which was associated with comparable expression levels of *Sox9* and *Col2a1* between the two groups (Fig. 7*B*). Consistent with this, immunohistochemical analysis of metatarsals revealed that expression levels of Sox9 and Col2a1 were not altered by treatment with FGF23/sKL (Fig. 7, *C* and *D*), indicating that impaired proliferation of chondrocytes in the proliferating zone is unlikely to be caused by impaired transition of resting chondrocytes into proliferating chondrocytes. Next, we investigated whether maturation of hypertrophic chondrocytes was affected by FGF23/sKL treatment. *In situ* hybridization and real-time RT-PCR analyses demonstrated the decreased expression of *Col10a1* in metatarsals treated with FGF23/sKL (Fig. 8, *A* and *B*). FGF23/sKL did not show any effect on *Col10a1* expression in primary chondrocytes (Fig. 8*C*), suggesting that the effect of FGF23/sKL on decreased *Col10a1* expression is unlikely due to the direct action of FGF23/sKL on hypertrophic chondrocytes. Interestingly, calcium deposition in the hypertrophic zone was impaired in metatarsals with FGF23/sKL (Fig. 8, *D* and *E*), indicating that FGF23/sKL delays maturation of hypertrophic chondrocytes.

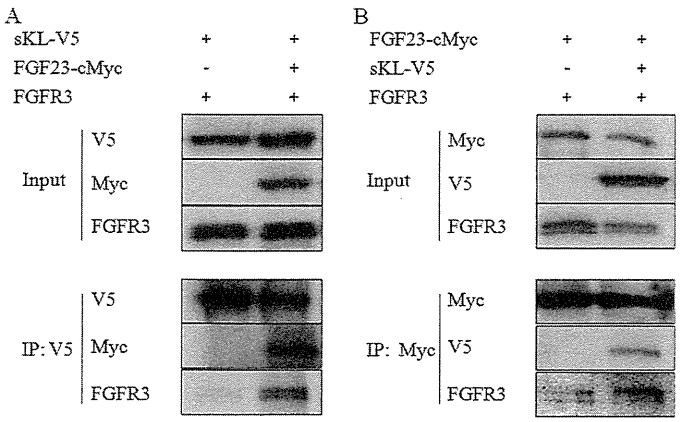


FIGURE 5. **Interaction between FGF23 and FGFR3 is enhanced in the presence of sKL.** *A*, HEK293 cells were transfected with FGFR3 and sKL-V5 expression vectors in the presence or absence of FGF23-cMyc expression vector. Immunoprecipitation with V5 was followed by Western blot analysis for cMyc and FGFR3. *B*, HEK293 cells were transfected with FGFR3 and FGF23-cMyc expression vectors in the presence or absence of sKL-V5 expression vector. Immunoprecipitation with cMyc was followed by Western blot analysis for V5 and FGFR3. The figures shown are the representative from at least three independent experiments.

*FGF23 Suppresses Indian Hedgehog Expression in the Presence of sKL*—To further analyze the mechanisms whereby FGF23/sKL signaling impairs chondrocyte proliferation, we examined the expression of Indian hedgehog (Ihh) because Ihh is well known to be involved in chondrocyte proliferation and activation of FGFR3 signaling has been shown to result in decreased expression of Ihh (21–25). *Ihh* expression was significantly lower in primary chondrocytes and metatarsals treated with FGF23/sKL than that in controls (Fig. 9*A*). In line with

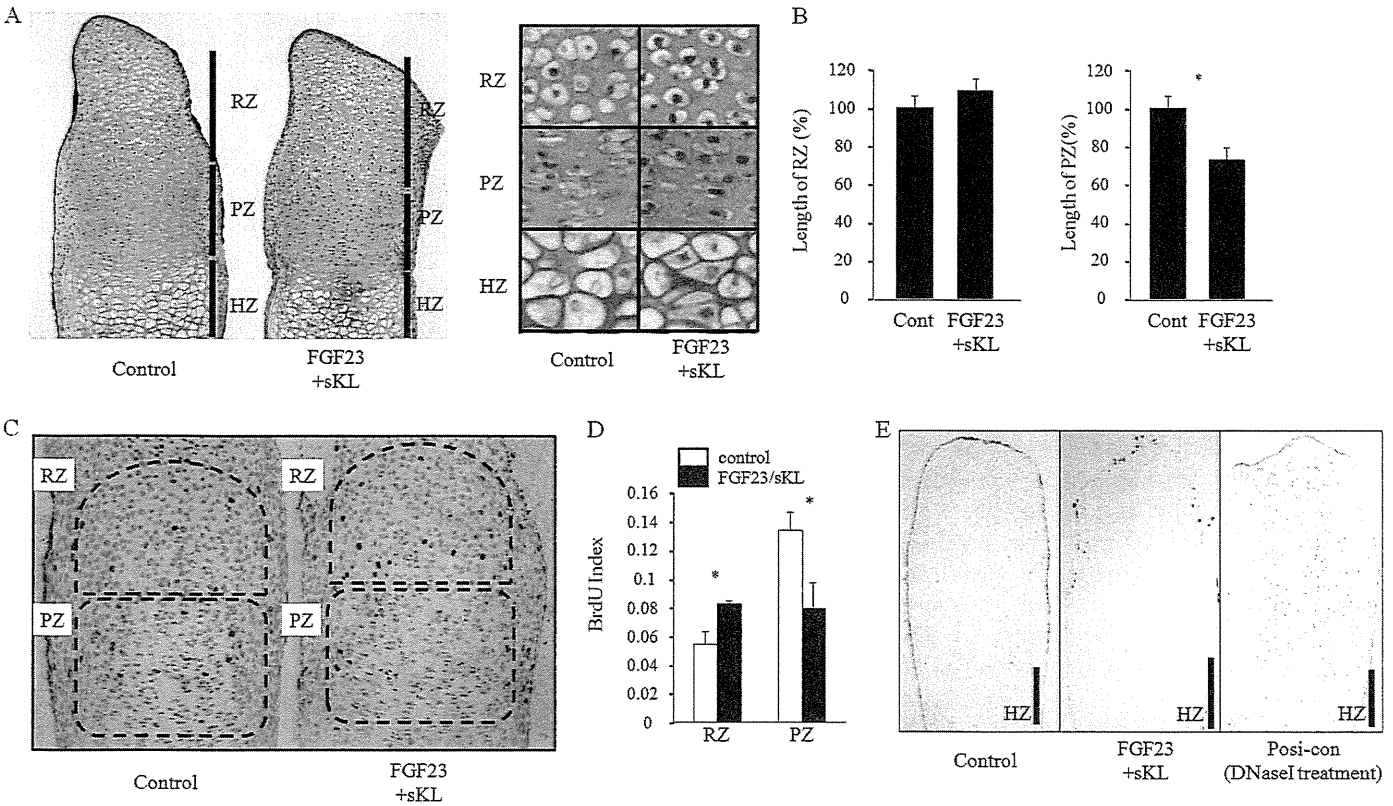


FIGURE 6. **FGF23 suppresses chondrocyte proliferation in the proliferating zone in the presence of sKL.** *A* and *B*, metatarsals were cultured for 12 days with or without FGF23 (300 ng/ml) and sKL (300 ng/ml). Paraffin-embedded sections were subjected to Hematoxylin and Eosin staining (*A*) and lengths of resting and proliferating zones were determined ($n = 5$) (*B*). *C–E*, metatarsals were cultured for 6 days with or without FGF23 (300 ng/ml) and sKL (300 ng/ml). BrdU staining (*C*) and TUNEL staining (*E*) were performed. The ratio of BrdU-positive cells over total cells was calculated (referred as BrdU index) ($n = 3–5$) (*D*). The figures shown are the representative from at least three independent experiments. The values were expressed as mean ± S.E. *, $p < 0.05$.